

Unveiling the physical conditions in NGC 6910

HARMEEN KAUR,¹ SAURABH SHARMA,² LOKESH K. DEWANGAN,³ DEVENDRA K. OJHA,⁴ ALOK DURGAPAL,¹ AND NEELAM PANWAR²

¹*Center of Advanced Study, Department of Physics
DSB Campus, Kumaun University Nainital, 263002, India*

²*Aryabhatta Research Institute of Observational Sciences (ARIES), Manora Peak, Nainital 263 002, India*

³*Physical Research Laboratory, Navrangpura, Ahmedabad - 380 009, India*

⁴*Tata Institute of Fundamental Research (TIFR), Homi Bhabha Road, Colaba, Mumbai - 400 005, India*

(Received —, 2020; Revised —, 2020; Accepted —, 2020)

Submitted to ApJ

ABSTRACT

Deep and wide-field optical photometric observations along with multiwavelength archival datasets have been employed to study the physical properties of the cluster NGC 6910. The study also examines the impact of massive stars to their environment. The age, distance and reddening of the cluster are estimated to be ~ 4.5 Myr, 1.72 ± 0.08 kpc, and $E(B - V)_{min} = 0.95$ mag, respectively. The mass function slope ($\Gamma = -0.74 \pm 0.15$ in the cluster region is found to be flatter than the Salpeter value (-1.35), indicating the presence of excess number of massive stars. The cluster also shows mass segregation towards the central region due to their formation processes. The distribution of warm dust emission is investigated towards the central region of the cluster, showing the signature of the impact of massive stars within the cluster region. Radio continuum clumps powered by massive B-type stars (age range ~ 0.07 - 0.12 Myr) are traced, which are located away from the center of the stellar cluster NGC 6910 (age ~ 4.5 Myr). Based on the values of different pressure components exerted by massive stars, the photoionized gas associated with the cluster is found to be the dominant feedback mechanism in the cluster. Overall, the massive stars in the cluster might have triggered the birth of young massive B-type stars in the cluster. This argument is supported with evidence of the observed age gradient between the cluster and the powering sources of the radio clumps.

Keywords: open clusters and associations: individual (NGC 6910); stars: kinematics and dynamics; stars: luminosity function, mass function; stars: formation

1. INTRODUCTION

Massive stars ($\geq 8 M_{\odot}$) are regarded as powerful agents which can significantly affect their host molecular cloud through their photoionized gas and/or stellar winds. The impact of energetic feedback from massive stars can trigger new generation of young protostars. However, understanding the feedback mechanism of massive OB stars is still under debate (Zinnecker & Yorke 2007; Tan et al. 2014). In this context, young open clusters (age < 10 Myr) are thought to be a unique laboratory for understanding the processes of star-formation as they harbor both low-mass and high-mass stars of very young ages. Young open clusters, just formed from the gravitationally bound molecular clouds and still embedded in the parent nebulous regions, contains dust and gas. The study of the ionized gas, dust (cold and warm) emission, and molecular gas can give us observational clues about the physical processes that govern their formation (Bastian et al. 2010; Deharveng et al. 2015).

Furthermore, the investigation of young open clusters offers to study the initial mass function (IMF) of stellar objects, which is an important statistical tool to understand the formation of stars (Sharma et al. 2017; Jose et al.

2017; Panwar et al. 2018, and references therein). It is supported with the fact that young open clusters host a broad mass range of cluster members, which can also be used to quantify the relative numbers of stars in different mass bins and to constrain the IMF.

A few examples exist in literature (see e.g. Pandey et al. 2001, 2005; Sharma et al. 2007, 2008; Jose et al. 2017), showing change in the slope of the mass function (MF) as a function of radial distance from the cluster center in a sense that the central region has more number of massive stars as compared to the outer regions. Hence, in cases of young clusters, it indicates the imprint of the star-formation process, while in old clusters it may be due to dynamical evolution of the clusters. Massive systems sink towards the center, allowing to gain more potential energy which heats the cluster. The time scale for this mass segregation to complete is not very well known. It is considered as an active area of research, especially because of the need to understand trapezium-like sub-systems in star clusters (Mermilliod 2000), and the associated implications for the formation mechanisms of massive stars (Bonnell et al. 1998).

Therefore, with the aim to investigate the stellar IMF as well as the physical processes governing the interaction and feedback effect of massive stars in their vicinity, we have selected a promising young cluster NGC 6910. This cluster is believed to host at least ten massive stars of spectral type B2V-O9V (e.g., Reipurth & Schneider 2008). However, the rich population of massive stars in this cluster and their effects on the surrounding field are largely unexplored and deserve a systematic study. To the best of our knowledge, no comprehensive observational investigation of a large-scale area around NGC 6910 is available in the literature. In order to compute the age and distance of the cluster, in this paper we present new deep, wide-field, and multiband ($UBV(RI)_c$) photometry around NGC 6910. Furthermore, we have also examined the distribution of massive stars, ionized gas, and warm dust emission in the cluster using multiwavelength data sets.

The structure of the paper is as follow. In Section 2, a brief overview of this region is presented. Section 3 provides details of new optical observations and reduction procedures along with the available data sets from various archives. In Section 4, we study the structure of this cluster. In this section, we also discuss the basic parameters of cluster (i.e. reddening law, extinction, distance), derived MF slope in the region, and explored the physical environment around the cluster including feedback effects from the massive stars. Finally, Section 5 summarizes the various results.

2. OVERVIEW OF THE NGC 6910 CLUSTER

The NGC 6910 cluster was discovered in 1786 by William Herschel and many photometric studies of the cluster members have been presented later (for details, cf. Reipurth & Schneider 2008). The distance to NGC 6910 amounts to about 1.5 kpc (Davies & Tovmassian 1963; Becker & Fenkart 1971; Battinelli & Capuzzo-Dolcetta 1991; Dambis 1999), placing it behind the Cygnus Rift, within the Local (Orion) spiral arm of the Galaxy. In consequence, the average color-excess of the cluster members, $E(B-V)$, is found to be of the order of 1 mag and varies across the cluster (Turner 1976). The age of the cluster was estimated to be in the range between 5 Myr and 10 Myr (Davies & Tovmassian 1963; Harris 1976; Battinelli & Capuzzo-Dolcetta 1991; Delgado & Alfaro 2000).

The NGC 6910 cluster is part of a complex of actively star-forming molecular clouds and young clusters, the Cygnus X region, which is extended over $\sim 7^\circ \times 7^\circ$ area and located at a distance of about 1.7 kpc (Reipurth & Schneider 2008). Several OB stars in Cygnus X have been grouped into nine OB associations by Humphreys (1978) and the famous Cyg OB2 association is the most massive among them, which contains several thousand OB stars and is analogous to the young globular clusters in the large Magellanic cloud (Reddish et al. 1966; Massey & Thompson 1991). OB associations in Cygnus X region are among the largest groups of O-type stars known in our Galaxy, and can strongly influence their entire surrounding field. In Figure 1, we show the color-composite of the $4^\circ \times 4^\circ$ field-of-view (FOV) of Cygnus X region containing NGC 6910 (see a solid black box) obtained by using 1.4 GHz Canadian Galactic Plane Survey (CGPS) image, 12 μm Wide-field Infrared Survey Explorer (*WISE*) image, and 115 GHz image (Dame et al. 2001). The approximate location of OB associations are also shown as white ellipses (cf. Humphreys 1978; Schneider et al. 2006, 2007). The images at 1.4 GHz and 115 GHz represent the distribution of the ionized emission and the molecular gas emission, respectively, while the *WISE* 12 μm image covers the prominent polycyclic aromatic hydrocarbon (PAH) features at 11.3 μm , indicative of photo-dissociation regions (or photon-dominated regions, or PDRs). The entire complex seems to contain PAH features produced under the influence of massive stars. The cluster NGC 6910 is spatially seen at the border of a dominate circular red region called as ‘ γ Cygni supernova remnant (SNR)’ (G78.2+2.1; see Figure 1 in Tibaldo & Grenier 2013). The γ Cygni SNR is characterized as a typical shell-type SNR (e.g., Uchiyama et al. 2002; Piano et al. 2019), and is located at a distance of ~ 1.5 kpc (Landecker et al. 1980). A Herbig Ae/Be star BD+40° 4124 (Sandell et al. 2012) is also seen towards the north-west direction of this cluster.

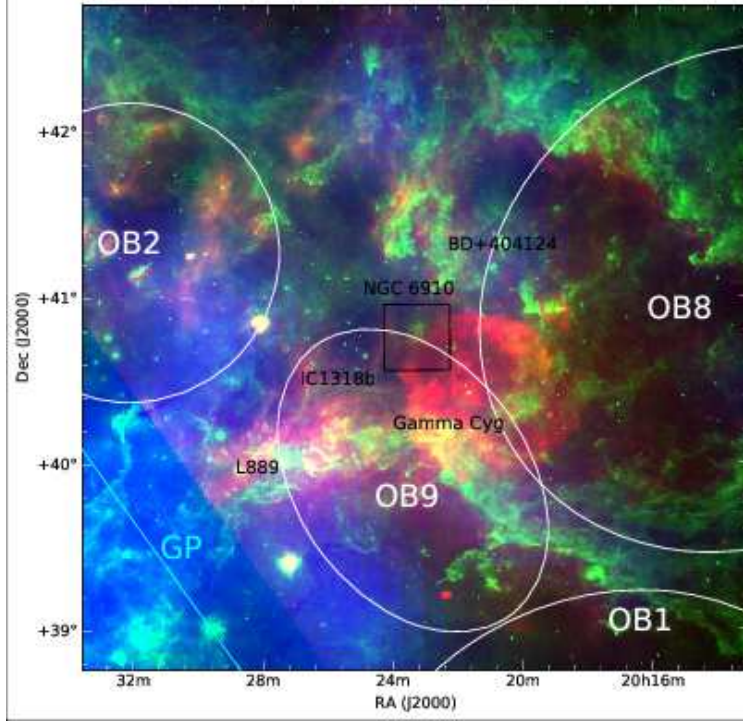


Figure 1. Color-composite image of the 4×4 degree² FOV of Cygnus X region containing NGC 6910 (black box) obtained by using 1.4 GHz (red, CGPS), $12 \mu\text{m}$ (green, *WISE*) and 115 GHz (blue, Dame et al. (2001)) images. Locations of different OB associations (white ellipses) are also shown in the figure (cf. Humphreys 1978; Schneider et al. 2006, 2007).

The NGC 6910 cluster is located in the outskirts of the IC 1318 b/c bright nebula, somewhat within the Cygnus OB9 association of $30 \text{ pc} \times 40 \text{ pc}$ size containing numerous massive young stars. The IC 1318 b/c regions are part of a single, giant H II region, prominent in the radio domain (Baars & Wendker 1981) and bifurcated by a massive, highly structured, dust lane ‘L889’ (Dickel et al. 1977; Wendker et al. 1983). A possible ionizing source of the IC 1318 b/c nebula is an O9V type star names as ‘GSC 03156-00657’ (Arhipova & Lozinskaia 1978; Appenzeller & Wendker 1980). However, this star is not a member of NGC 6910, because it is located away from the cluster center. The precise relation between the NGC 6910 cluster and the H II region is unclear. Also, this cluster has been known to contain at least 40 stars showing H α in emission, around 12 pre-main sequence (PMS) stars, and 10 massive stars (Melikian & Shevchenko 1990; Shevchenko et al. 1991; Delgado & Alfaro 2000; Kubát et al. 2007; Reipurth & Schneider 2008), which makes it an ideal site to investigate star-formation activities.

3. OBSERVATION AND DATA REDUCTION

3.1. Optical data

The optical CCD $UBV(RI)_c$ photometric data of the NGC 6910 region, centered at α_{J2000} : $20^{\text{h}}23^{\text{m}}12^{\text{s}}$, δ_{J2000} : $+40^{\circ}46'42''$; $l = 78^{\circ}.683$ and $b^{\circ} = 2.013$, were acquired by using the 2048×2048 pixel² CCD camera mounted on the f/13 Cassegrain focus of the 104-cm Sampurnanand telescope of Aryabhata Research Institute of Observational Sciences (ARIES), Nainital, India. In this set up, each pixel of the CCD corresponds to 0.37 arcsec and the entire chip covers a FOV of $\sim 13 \times 13$ arcmin² on the sky. We have carried out observations of this cluster in four pointings covering a total FOV of 22×23 arcmin² as shown in Figure 2. To improve the signal to noise ratio (SNR), the observations were carried out in the binning mode of 2×2 pixels. The read-out noise and gain of the CCD are $5.3 e^-$ and $10 e^-/\text{ADU}$ respectively. The average FWHMs of the star images were ~ 3 arcsec. A number of bias frames and twilight-flat frames were also taken during observations. A number of short and deep (long) exposure frames were taken to observe both bright and faints stars in the field. The complete log of the observations is given in Table 1.

The CCD data frames were reduced by using the computing facilities available at the Center of Advanced Study, Department of Physics, Kumaun University, and ARIES, both located in Nainital, India. Initial processing of the data

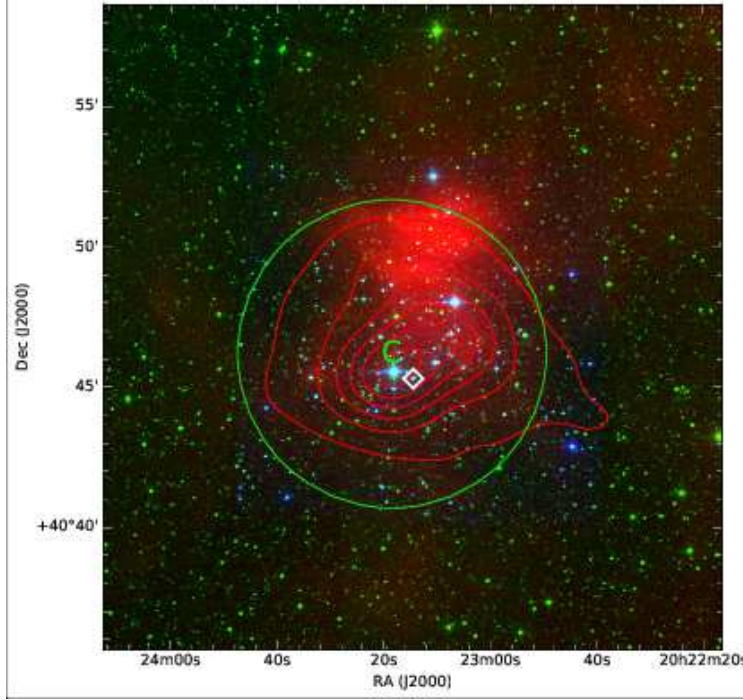


Figure 2. Color-composite image obtained by using the $22\ \mu\text{m}$ (red, *WISE*), $2.2\ \mu\text{m}$ (green, *2MASS*) and $0.55\ \mu\text{m}$ (blue, present study) images for an area of $\sim 22 \times 23\ \text{arcmin}^2$ around NGC 6910 cluster. Red contours are the surface density contours, whereas the green circle shows the cluster boundary (cf. Section 4.1.1). White diamond is the location of massive O9.5 star (BD+40 4148) reported in this region (Reipurth & Schneider 2008).

frames was done by using the IRAF¹ and ESO-MIDAS² data reduction packages. Photometry of the cleaned frames were carried out by using DAOPHOT-II software (Stetson 1987). The point spread function (PSF) was obtained for each frame by using several isolated stars. Magnitudes obtained from different frames were averaged. When brighter stars were saturated on deep exposure frames, their magnitudes were taken from short exposure frames. We used the DAOGROW program (Stetson 1990) for construction of an aperture growth curve required for determining the difference between the aperture and profile-fitting magnitudes. Calibration of the instrumental magnitudes to the standard system was done by using the procedures outlined by Stetson (1992). The broad-band $UBV(RI)_c$ observations of the NGC 6910 region were standardized by observing stars in the SA98 field (Landolt 1992) centered at $\alpha_{J2000}: 06^h52^m12^s$, $\delta_{J2000}: -00^\circ19'17''$. The calibration equations derived by using the standard stars in the SA98 field by the least-squares linear regression are as follows:

$$u = U + (6.771 \pm 0.003) - (0.009 \pm 0.002)(U - B) + (0.677 \pm 0.005)X \quad (1)$$

$$b = B + (4.548 \pm 0.002) + (0.008 \pm 0.001)(B - V) + (0.407 \pm 0.003)X \quad (2)$$

$$v = V + (4.149 \pm 0.002) - (0.046 \pm 0.002)(V - I_c) + (0.256 \pm 0.003)X \quad (3)$$

$$r_c = R_c + (4.046 \pm 0.002) - (0.013 \pm 0.001)(V - R_c) + (0.190 \pm 0.003)X \quad (4)$$

$$i_c = I_+ (4.559 \pm 0.004) - (0.017 \pm 0.001)(V - I_c) + (0.135 \pm 0.006)X \quad (5)$$

¹IRAF is distributed by National Optical Astronomy Observatories, USA

²ESO-MIDAS is developed and maintained by the European Southern Observatory.

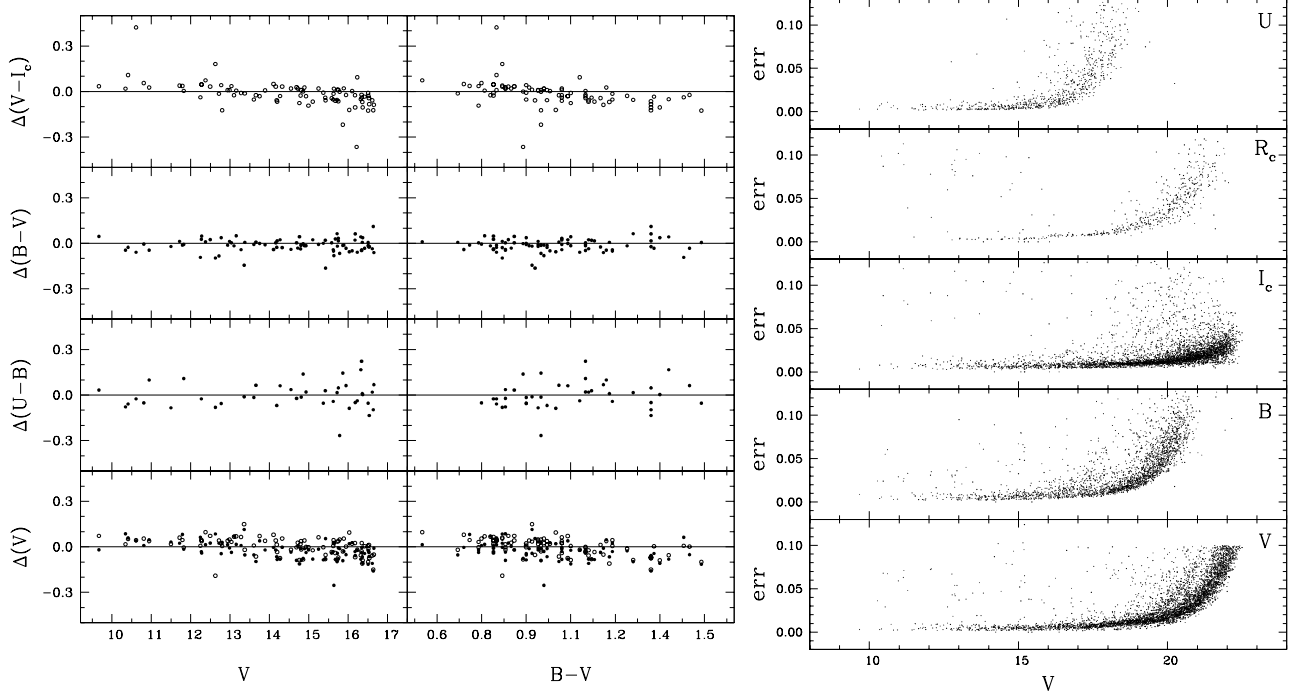


Figure 3. *Left panel:* Comparison of the present CCD photometry with those available in literature as a function of present V magnitudes and $(B - V)$ colors. Dots and circles represent data from Delgado & Alfaro (2000, UBV) and Kolaczowski et al. (2004, VI), respectively. *Right panel:* Photometric errors as a function of V magnitude in different filters.

where U, B, V, R_c and I_c are the standard magnitudes and u, b, v, r_c and i_c are the instrumental aperture magnitudes, which are normalized per second of exposure time and X is the airmass. In the cluster field, we have generated secondary standards by applying the above equations to the stars which were observed in the same night as the standard field. Then, we calibrated all the stars in different subregions of the cluster field which were observed during different nights by applying the off-set between the instrumental and standard magnitudes of the secondary standards. We have carried out a comparison of the present calibrated data with those CCD data ($V < 17$ mag) present in the literature i.e., Delgado & Alfaro (2000, UBV) and Kolaczowski et al. (2004, VI). The difference Δ (present – literature) as a function of present V magnitudes and $(B - V)$ colors is shown in the left panel of Figure 3. Although, there is some trend in the difference of V mags and $V - I_c$ colors in the range of 11 to 16 mag in V band, but the scatter is small and the effect will be minimal to the scientific results of this study. The comparison indicates that the magnitudes and colors obtained in the present work are in fairly agreement with those available in literature. The typical DAOPHOT errors in different bands as a function of V magnitudes are shown in the right panel of Figure 3. It can be seen that the errors become large (> 0.1 mag) for fainter magnitudes and were not used in the present analysis. In this study a total of 4638 sources have been identified with detections at least in V and I_c bands and having photometric error less than 0.1 mag upto $V \simeq 22$ mag.

The above optical photometry which will be further used for our analysis, can be incomplete due to various reasons, e.g., nebulosity, crowding of the stars, detection limit etc. In particular it is very important to know the completeness limits in terms of mass to derive correct MF slopes. The IRAF routine ADDSTAR of DAOPHOT II was used to determine the completeness factor (CF). In this method, artificial stars of known magnitudes and positions are randomly added in the original frames and then these artificially generated frames are re-reduced by the same procedure as used in the original reduction. The ratio of the number of stars recovered to those added in each magnitude gives the CF as a function of magnitude. We followed the procedure given by Sagar & Richtler (1991). We added artificial stars to both V and I images in such a way that they have similar location geometrically but differ in I brightness according to mean $(V - I)$ colors of the main sequence stars. The luminosity distribution of artificial stars are in such a way that more stars are inserted at fainter magnitude bins. A number of independent sets of artificial stars are inserted into a given data frames for the determination of the CF. In all about 15% of the total stars are added so that crowding characteristics of the original frame do not change significantly (see, Sagar & Richtler 1991). The minimum

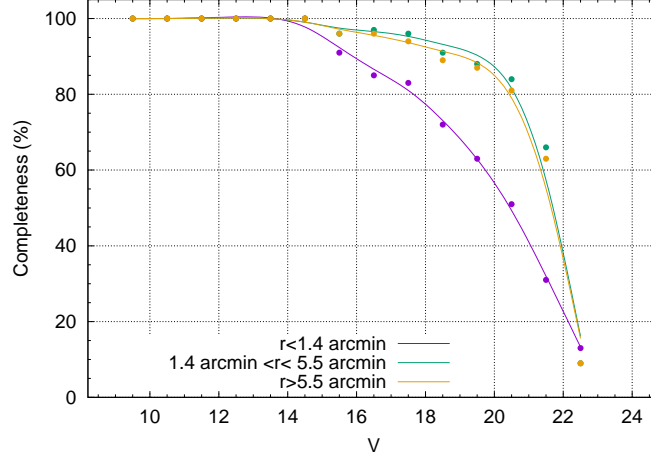


Figure 4. Completeness factor as a function of V magnitude derived from the artificial star experiment *ADDSTAR*.

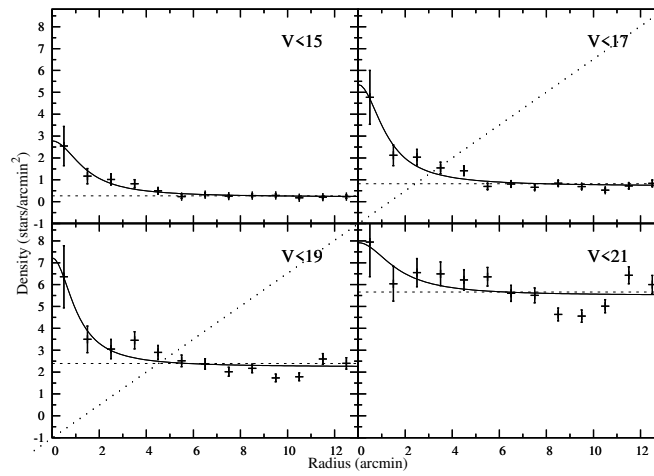


Figure 5. Radial density profiles of the NGC 6910 cluster at different magnitude levels using the present optical data. The solid curve shows a least-squares fit of King (1962) profile to the observed data points. The error bars represent $1/\sqrt{N}$ errors. The horizontal line indicates the density of field stars.

value of the CF in V and I bands is used to correct the data incompleteness (see, Sagar & Richtler 1991). The CF for different regions of the NGC 6910 cluster are shown in Figure 4. As expected, we found that the incompleteness of the data increases with increasing magnitude and increasing stellar density (i.e. towards core of cluster, cf. Section 4.1.1). In this study, our data in the cluster region is found to be 80% complete upto 20.6 mag in V band, corresponding to a mass completeness limit of $0.8 M_{\odot}$ for observed distance of 1.72 kpc and $E(B - V) = 0.95$ mag (cf. Section 4.1.4).

3.2. Archival data sets

We have also used the archival near-infrared (NIR), mid-infrared (MIR) and radio data of the selected region as observed in optical bands for our analysis. Brief description of these is given in Table 2. The processed *Herschel* temperature and column density ($N(\text{H}_2)$) maps (resolution $\sim 12''$) have been utilized in this work, which were downloaded from the publicly available site¹. These maps were generated as a part of the EU-funded ViaLactea project (Molinari et al. 2010). The Bayesian *Point Process MAPping* (PPMAP) procedure (Marsh et al. 2015) was adopted for producing these *Herschel* maps (see also Marsh et al. 2017).

4. RESULTS AND DISCUSSION

¹<http://www.astro.cardiff.ac.uk/research/ViaLactea/>

4.1. Cluster's physical properties

4.1.1. Extent and structure of the cluster

The initial stellar distribution in star clusters may be governed by the structure of the parental molecular cloud and also how star-formation proceeds in the cloud. Later evolution of the cluster may be governed by the internal gravitational interaction among member stars and external tidal forces due to the Galactic disc or giant molecular clouds (Chen et al. 2004; Sharma et al. 2006). The structure and radius of the NGC 6910 cluster (core and corona regions) can be studied by means of density estimations. Since the distribution of stars in a cluster follows a systematic distribution from the cluster to the field region, the center of the cluster is estimated by involving a Gaussian kernel with the stellar distribution and taking the point of maximum density as the center. This was performed for both axes to get the center coordinates of the cluster i.e., α_{J2000} : $20^h23^m18^s$, δ_{J2000} : $+40^\circ46'12''$. To determine the radial stellar surface density, the cluster was divided into number of concentric rings. The projected radial stellar density in each concentric circle was obtained by dividing the number of stars in each annulus by its area, and this is plotted in Figure 5 for various magnitudes levels. The error bars are derived assuming that the number of stars in each annulus follows Poisson statistics. The point where the radial density becomes nearly constant and merges with the contaminating field star density (indicated by horizontal dashed lines in the plot) is defined as the radius of the cluster ' r_{cl} ' (see also, Sharma et al. 2006). For almost all magnitude levels, we can determine the r_{cl} of this cluster as 5.5 arcmin. The observed radial density profile (RDP) of the cluster was parameterized following the approach by Kaluzny & Udalski (1992) in which the projected radial density $\rho(r)$ is described as

$$\rho(r) \propto \frac{f_0}{1 + \left(\frac{r}{r_c}\right)^2} \quad (6)$$

where the cluster's core radius ' r_c ' is the radial distance at which the value of projected radial density ' $\rho(r)$ ' becomes half of the central density ' f_0 '. Within uncertainties, the King-model (King 1962) reproduces well the radial density profile of the cluster at different magnitude levels except for $V < 21$ mag. This might be due to the apparent contamination in the cluster region from the field stars at fainter magnitudes. By fitting the King-model surface density profile to the observed RDP of stars with $V \simeq 19$ mag having least fitting error, we have found that the core radius of this cluster comes out as 1.4 arcmin.

To further study the structure of the cluster and stellar density distribution in the region, we generated stellar surface density maps using the nearest neighbor (NN) method as described by Gutermuth et al. (2005). We have taken the radial distance necessary to encompass the 20th nearest star detected in optical band ($V < 16$ mag) and computed the local surface density in a grid size of ~ 20 arcsec. Surface density contours in the NGC 6910 region are shown in the Figure 2 as red contours, whereas, the cluster region as determined by RDP is shown as a green circle. The lowest contour is 1σ above the mean of stellar density (i.e. 1.3 ± 2.2 stars/pc² at 1720 pc) and the step size is equal to the 1σ (2.2 stars/pc² at 1720 pc). Figure 2 reveals that stellar surface density contours correspond to the cluster size (5.5 arcmin) determined by the RDP. The core region of this cluster seems to be elongated.

4.1.2. Cluster membership of stellar sources

Membership determination based on proper motion (PM) studies will be useful to carry out astrophysical studies in the region of the cluster. To determine the membership probability, we adopted the method described in Balaguer-Núñez et al. (1998) by using *Gaia* PM data (cf. Table 2). This method has been previously used for ω Centauri (Bellini et al. 2009), NGC 6809 (Sariya et al. 2012), NGC 6366 (Sariya & Yadav 2015) and for NGC 3201 (Sariya et al. 2017). In Figure 6 (left panel), we show the PMs $\mu_\alpha \cos(\delta)$ and μ_δ vector point diagrams (VPDs: top panels) and the corresponding G versus $(G_{BP} - G_{RP})$ color-magnitude diagrams (CMDs: bottom panels) for the stars located within the radius of the cluster i.e., $r_{cl} < 5.5$ arcmin. The left sub-panel show all stars, while the middle and right sub-panels show the probable cluster members and field stars respectively. A tight circular clump can be seen visually at $\mu_{xc} = -3.4$ mas yr⁻¹, $\mu_{yc} = -5.4$ mas yr⁻¹ having radius of 0.8 mas yr⁻¹ in the top-left sub-panel of Figure 6. As we know that the cluster stars have more or less similar PMs, this group most probably represents the PMs of cluster stars. The chosen radius is a compromise between losing cluster members with poor PMs and including field stars sharing the cluster mean PM. The corresponding a well defined CMD of these most probable cluster members can be seen in the lower-middle sub-panel. The remaining stars in the VPD are assigned as field stars which is further demonstrated by the broad distribution in their CMD (lower-right sub-panel). Few cluster members might be visible in this CMD because of their wrong estimation of PMs due to large errors in their values. Assuming a distance of 1.74

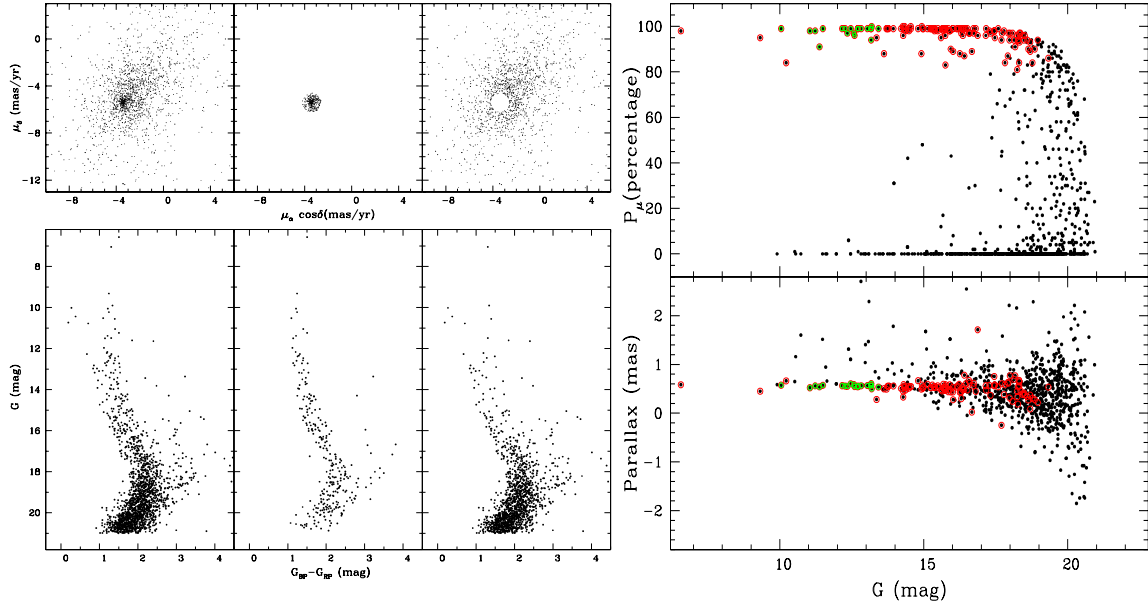


Figure 6. *Left panel:* Proper motion vector-point diagrams (VPDs; top sub-panels) and *Gaia* DR2 G vs. $(G_{BP} - G_{RP})$ CMDs (bottom panels). The left sub-panels show all stars, while the middle and right sub-panels show the probable cluster members and field stars. *Right panel:* Membership probability P_μ and Parallax values as a function of G magnitude for stars in cluster region. Green circles have parallax error less than 0.05 mas and red circles have membership probability greater than 80 percent and $G < 20$ mag.

kpc (Delgado & Alfaro 2000) and a radial velocity dispersion of 1 km s^{-1} for open clusters (Girard et al. 1989), the expected dispersion (σ_c) in PMs would be $\sim 0.12 \text{ mas yr}^{-1}$. For remaining field stars we have calculated: $\mu_{xf} = -2.2 \text{ mas yr}^{-1}$, $\sigma_{xf} = 3.9 \text{ mas yr}^{-1}$ and $\mu_{yf} = -4.6 \text{ mas yr}^{-1}$, $\sigma_{yf} = 4.3 \text{ mas yr}^{-1}$, as the mean and standard deviation of their PM values in right ascension and declination axes, respectively. These values are further used to construct the frequency distributions of cluster stars (ϕ_c^ν) and field stars (ϕ_f^ν) by using the equations given in Yadav et al. (2013) and then the value of membership probability (ratio of distribution of cluster stars with all the stars) by using the following equation:

$$P_\mu(i) = \frac{n_c \times \phi_c^\nu(i)}{n_c \times \phi_c^\nu(i) + n_f \times \phi_f^\nu(i)} \quad (7)$$

where n_c ($=0.16$) and n_f ($=0.84$) are the normalized numbers of stars for the cluster and field region ($n_c + n_f = 1$).

The estimated membership probability of the *Gaia* sources located within the radius of the NGC 6910 cluster region is plotted as a function of G magnitude in Figure 6 (right panel). As can be seen in this plot, a high membership probability ($P_\mu > 80$ percent) extends down to $G \sim 20$ mag. At fainter magnitudes the probability gradually decreases. In Figure 6 (right panel), we have also plotted parallax of the same stars as a function of G magnitude. Except few outliers, most of the stars with high membership probability ($P_\mu > 80$ percent and $G < 20$ mag) are following a tight distribution. Finally, from the above analysis, we calculate membership probability of 916 stars in the NGC 6910 cluster region, and 128 stars were assigned as cluster members based on their high membership probability ($P_\mu > 80$ percent and $G < 20$ mag). The details of these cluster members are given in Table 3.

4.1.3. Reddening law in the region

The nature of diffuse interstellar medium (ISM) is often characterized by the ratio of total-to-selective extinction, represented by $R_V = A_V/E(B - V)$. The normal reddening law for the solar vicinity gives the value $R_V = 3.1 \pm 0.2$ (Whittet 2003; Guetter & Vrba 1989; Lim et al. 2011), but in the case of several star-forming regions having an unusual distribution of dust sizes, it is found to be abruptly high (see e.g., Pandey et al. 2000, 2008; Hur et al. 2012; Pandey et al. 2013; Kumar et al. 2014). To separate the influence of normal extinction produced by the general ISM from that of abnormal extinction arising within regions, we used $(V - \lambda)$ versus $(B - V)$ two-color diagrams (TCDs) (cf., Chini et al. 1990; Pandey et al. 2000, 2003), where λ indicates one of the wavelengths of the broad-band filters

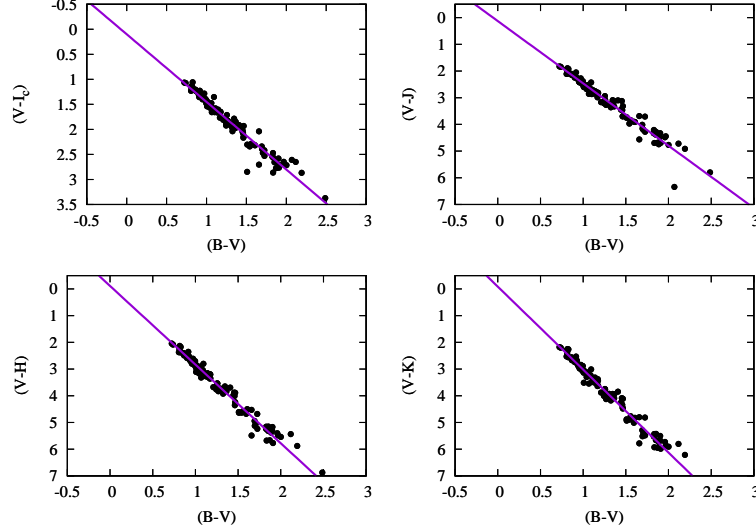


Figure 7. $(V - I_c)$, $(V - J)$, $(V - H)$, $(V - K)$ versus $(B - V)$ TCDs for the stellar sources associated with the NGC 6910 region (black dots, $P_\mu > 80\%$ and $G < 20$ mag) and straight lines show the least-square fit to the distribution of stars.

(J, H, K, I_C) . Figure 7 shows the $(V - \lambda)$ versus $(B - V)$ TCDs of all the cluster member stars having optical and NIR observations. The slopes of the least square fit to the distribution of stars in the $(V - I_c)$, $(V - J)$, $(V - H)$ and $(V - K)$ versus $(B - V)$ TCDs are found to be 1.35 ± 0.10 , 2.33 ± 0.12 , 2.94 ± 0.11 and 3.10 ± 0.09 , respectively, which are higher by a factor ‘ m ’ $\sim 1.21 \pm 0.01$ than those found for the general ISM (1.10, 1.96, 2.42 and 2.60; cf., Pandey et al. 2003). This concede a higher value for R_V ($\sim 3.75 \pm 0.02$, please refer Pandey et al. 2003, for detailed description on reddening law estimation), indicating larger grain sizes of the material in this region as compared to the general ISM. We have also calculated the R_V value for the stars which are not cluster members (i.e. $P_\mu < 20$ per cent and $V < 20$ mag) and found a similar value of R_V ($\sim 3.75 \pm 0.02$) as for cluster member stars. This means that, in general, the R_V value is higher in this region. Inside dense dark clouds, the coagulation due to grain collision and accretion of ice mantles on grains can change the size distribution leading to higher R_V values (Cardelli et al. 1989). In many star-forming regions, R_V values tend to diverge from the normal value towards the higher ones, for example: $R_V = 3.7$ (Kumar et al. 2014, the Carina region), $R_V = 3.3$ (Pandey et al. 2013, NGC 1931), $R_V = 3.5$ (Sharma et al. 2012, NGC 281) and $R_V = 3.7$ (Pandey et al. 2008, Be 59).

4.1.4. Extinction, distance and age of the cluster

The extinction towards the cluster NGC 6910 can be estimated by using the $(U - B)$ versus $(B - V)$ TCD as shown in the Figure 8 (left panel). In this figure, stars inside the cluster region ($r_{cl} < 5'.5$, black dots) along with intrinsic zero-age-main-sequence (ZAMS, blue dotted curve) taken from Pecaut & Mamajek (2013) are shown. We have also over-plotted the probable cluster members stars identified by using the PMs data (cf. Section 4.1.2) as red circles. The distribution of the stars shows a large spread along the reddening vector, indicating heavy differential reddening in this region. It reveals two different populations, one (mostly black dots) distributed along the ZAMS and another (mostly red circles) showing a large spread in their reddening value. The former having negligible reddening must be the foreground population and the latter could be member stars. If we look at the MIR images of this region (Figure 1), we see several dust lanes along with enhancements of nebular emission at many places. Both of them are likely responsible for the large spread of reddening in the NGC 6910 region. The ZAMS is shifted along the reddening vector with a slope of $E(U - B)/E(B - V) = 0.72 \times 1.21$ (corresponding to $R_V \sim 3.75$, cf. Section 4.1.3) to match the distribution of stars showing minimum reddening among the member population. Only those stars were chosen for reddening analysis if their position in the TCD indicated that their spectral type is A or earlier. This choice was dictated by several factors, such as, metallicity, distribution of binary stars, rotation, PMS stars and error in photometry (see for more detail, cf. Golay 1974; Phelps & Janes 1994). The cluster foreground reddening value, $E(B - V)_{min}$ thus comes out to be ~ 0.95 mag and the ZAMS reddened by this amount is shown by a red continuous curve. The other stars may be embedded in the nebulosity of this region and the maximum reddening

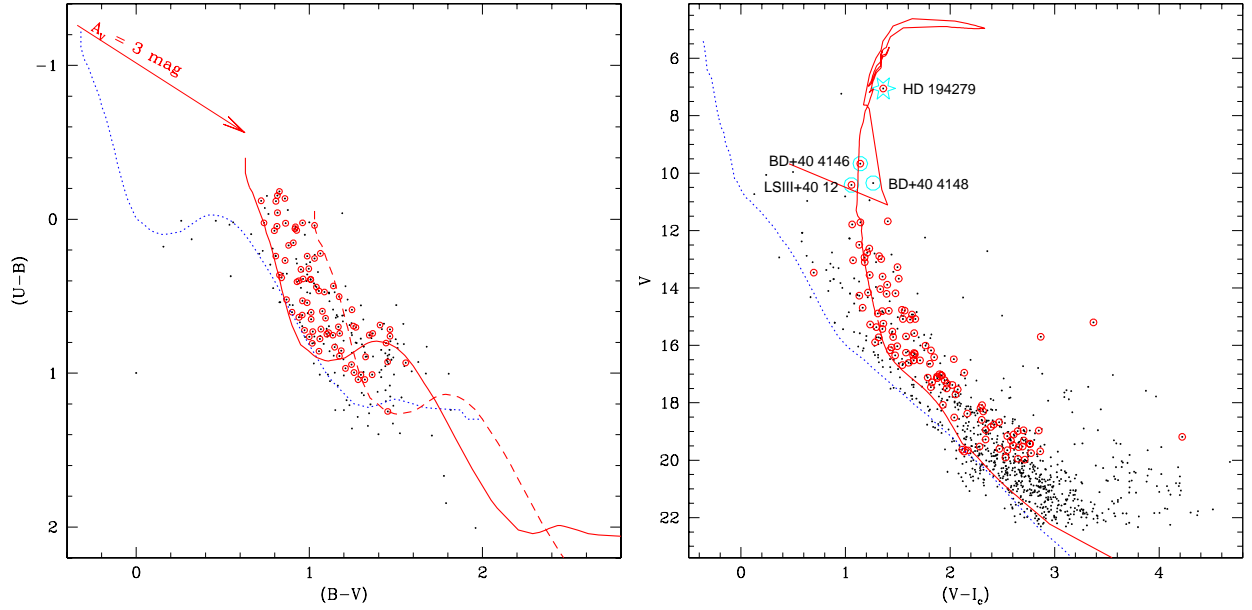


Figure 8. *Left panel:* $(U - B)$ vs. $(B - V)$ TCD for all the optically detected sources in the NGC 6910 region ($r_{cl} < 5.5'$). Red open circles are cluster member stars identified by their PMs data. The dotted blue curve represents the intrinsic Zero Age Main Sequence (ZAMS) for $Z = 0.02$ by Pecaut & Mamajek (2013). The continuous and dotted red curves represent ZAMS shifted along the reddening vector for $E(B - V) = 0.95 \text{ mag}$ and 1.35 mag , respectively. *Right panel:* V vs. $(V - I_c)$ CMD for similar sources. The ZAMS (Pecaut & Mamajek 2013, blue dotted curve corrected for the distance of 0.8 kpc) and post main-sequence isochrone for 4.5 Myr (Pastorelli et al. 2019, solid red curve corrected for the distance of 1.72 kpc and reddening $E(B - V) = 0.95 \text{ mag}$) are also shown.

value, $E(B - V)_{max}$ for them comes out to be 1.35 mag (dashed red curve). The approximate error in the reddening measurement ' $E(B - V)$ ' is $\sim 0.1 \text{ mag}$, and has been determined by the procedure outlined in Phelps & Janes (1994).

Photometric distance ($\sim 1.5 \text{ kpc}$) of this cluster has been estimated previously in the literature (Shevchenko et al. 1991; Vansevicius 1992). Recent distance estimates put this cluster at a distance of 1.6 kpc (Kolaczowski et al. 2004) to 1.74 kpc (Delgado & Alfaro 2000). Delgado & Alfaro (2000) have quoted the distance and age of this cluster as 1740 pc and 6.8 Myr, respectively. However, as the extinction in the NGC 6910 region is high and apparently anomalous, these distance measurements will be sensitive to the adopted R_V values. We calculated the distance of the member stars of this cluster by using their parallax values with good accuracy (error $< 0.05 \text{ mas}$) from Bailer-Jones et al. (2018). The mean distance value comes out to be $1.72 \pm 0.08 \text{ kpc}$. Distance and age of a cluster can also be derived quite accurately by using the CMD of their main-sequence (MS) member stars (cf. Phelps & Janes 1994; Sharma et al. 2006, 2017; Friel et al. 2014; Perren et al. 2015; Bossini et al. 2019; Pandey et al. 2020a,b). The V versus $(V - I)$ CMD for stars lying within the cluster region is shown in the right panel of Figure 8. The probable cluster member stars (cf. Section 4.1.2) are also plotted in the figure by red circles. Here also, the CMD reveals two different populations, one (mostly black dots) for foreground stars having almost zero reddening value (near dotted curve) and another (mostly red circles) for the cluster members at higher reddening value and larger distance. The CMD of cluster members displays a few MS stars upto $V=16 \text{ mag}$ and PMS stars at fainter end. The blue dotted curve in the right panel of Figure 8 denotes a ZAMS from Pecaut & Mamajek (2013), randomly corrected for a distance of 0.8 kpc, matches well with the distribution of foreground stars. We have further visually fitted the post-MS isochrone for an age of 4.5 Myr from Pastorelli et al. (2019) to the lower envelop of the distribution of member stars where the bend occurs in the MS. This choice of visual fitting was imposed by several factors, such as, distribution of binary stars, rotation and evolutionary effects (see for detail, cf. Golay 1974; Phelps & Janes 1994). It matches quite nicely which is corrected for a extinction value ' $E(B - V)_{min}=0.95 \text{ mag}$ ' as derived earlier in this section and a distance of 1.72 kpc (solid red curve). The locations of massive stars such as HD 194279 (B2Ia C, Blue super-giant; Adelman & Yüce 2007), BD+40 4148 (O9.5V; Hoag & Applequist 1965), BD+40 4146 (B1 D; Walker & Hodge 1968) and LS III +40 12 (B0.5V; Comerón & Pasquali 2012) are also matching well with the isochrone. Therefore, from both parallax and CMD analyses, we have derived the distance and post-MS age of this cluster as 1.72 kpc and 4.5 Myr, respectively.

The approximate error in the age estimation is ~ 2.5 Myr, as has been determined by the procedure outlined in [Phelps & Janes \(1994\)](#). A summary of physical parameters of the cluster is given in Table 4.

4.1.5. Mass function and dynamical age of the cluster

The distribution of stellar masses that form in one star-formation event in a given volume of space is called IMF and together with star-formation rate, it is one of the important statistical tools to study star-formation. The MF is often expressed by a power law, $N(\log m) \propto m^\Gamma$ and the slope of the MF is given as:

$$\Gamma = d \log N(\log m) / d \log m \quad (8)$$

where $N(\log m)$ is the number of stars per unit logarithmic mass interval. We have used our deep optical data to generate the MF of different regions of the NGC 6910 cluster as it reaches to the fainter end as compare to the *Gaia* DR2 data. For this, we have utilized the optical CMDs of the sources in the target region and that of the nearby field region of equal area and decontaminated the former sources from foreground/background stars and corrected for data in-completeness using a statistical subtraction method already described in details in our previous papers (cf. [Sharma et al. 2007, 2012, 2017](#); [Pandey et al. 2008, 2013](#); [Chauhan et al. 2011](#); [Jose et al. 2013](#)).

As an example, in Figure 9 (top-left panel) we have shown V versus $(V - I_c)$ CMDs for the stars lying within the cluster region in sub-panel ‘a’ and for those in the reference field region (taken as an annular area outside the cluster region having radius $5'.5 < r_{field} < 7'.65$) in sub-panel ‘b’. In sub-panel ‘c’, we have plotted the statistically cleaned V versus $(V - I_c)$ CMD for the cluster region which is showing the presence of PMS stars. Since, at the age of 4.5 Myr, the stars having $V \leq 16$ mag are considered to be still on the MS, for these stars the luminosity function was converted into MF using theoretical models by [Pastorelli et al. \(2019\)](#). The MF for the PMS stars was obtained by counting the number of stars in various mass bins (shown as evolutionary tracks) having age ≤ 7 Myr (age of cluster i.e. 4.5 Myr + error in age) in Figure 9 sub-panel ‘c’. The resulting MF of the cluster region by using MS ($2.3 < M/M_\odot < 24.86$) and MS+PMS ($0.8 < M/M_\odot < 24.86$) stars are plotted in Figure 9 (top-right) in upper and lower sub-panels, respectively. Similarly, we have also derived MF slopes ‘ Γ ’ for core and corona regions of the cluster using both MS and MS+PMS stars and their values are given in Table 5.

As the NGC 6910 cluster region contains several massive stars, we shall study the environment effects due to the presence of high mass stars on lower-mass end of the present day MF. In Figure 9 (top-right panel), we can observe that the MF for the cluster region shows a turn-off at $1.58 M_\odot$ and the distribution upto this mass limit can be represented by a single power law. The MF slopes of different regions of the cluster NGC 6910 are in general shallower than the Salpeter value ‘-1.35’, which indicates the abundance of massive stars in this cluster. It has been shown (see e.g. [Scalo 1986, 1998](#); [Kroupa 2002](#); [Chabrier 2003](#); [Corbelli et al. 2005](#)) that, for masses above $\sim 1 M_\odot$, the MF can generally be approximated by a declining power law with a slope similar to that found by [Salpeter \(1955\)](#). To investigate further, we look for the signature of mass-segregation in this cluster by checking the change of MF slope from the core region to the outer corona region of this cluster, which is in fact getting steeper in the outer corona region. To evaluate the degree-of-mass-segregation in the cluster, we subdivided the samples of cluster stars into two mass groups and plotted their cumulative distribution with respect to radial distance from the cluster center as shown in Figure 9 (bottom panels) for both MS (bottom-left panel) and MS+PMS (bottom-right panel) stars. Figure 9 (bottom panels) also reveals the effect of mass-segregation in the sense that relatively massive stars tend to lie near the cluster center. The Kolmogorov-Smirnov test confirms the above-mentioned mass-segregation at a confidence level better than $\sim 99\%$.

Dynamical relaxation is one of the possible reasons of the segregation of massive stars in the central region of this cluster. At the time of formation, the cluster may have a uniform spatial stellar mass distribution, however, the spatial stellar mass distribution would change with time as the cluster evolves dynamically. Low-mass stars in a cluster may possess high random velocities because of the dynamical relaxation; consequently, they will try to occupy a larger volume than the high mass stars and move away from the cluster center ([McNamara & Sekiguchi 1986](#); [Mathieu 1985](#)). To check whether mass-segregation is primordial or due to dynamical relaxation, we have estimated the dynamical relaxation time, ‘ T_E ’, the time in which individual stars exchange sufficient energy so that their velocity distribution approaches that of a Maxwellian equilibrium. The dynamical relaxation time is given by

$$T_E = \frac{8.9 \times 10^5 N^{1/2} R_h^{3/2}}{m^{1/2} \log(0.4N)} \quad (9)$$

where, $N = 215$ is the number of cluster members, $R_h = 1.6$ pc is the radius containing half of the cluster mass and $m = 4.31 M_\odot$ is the average mass of the cluster stars ([Spitzer & Hart 1971](#)). The total number of MS stars and

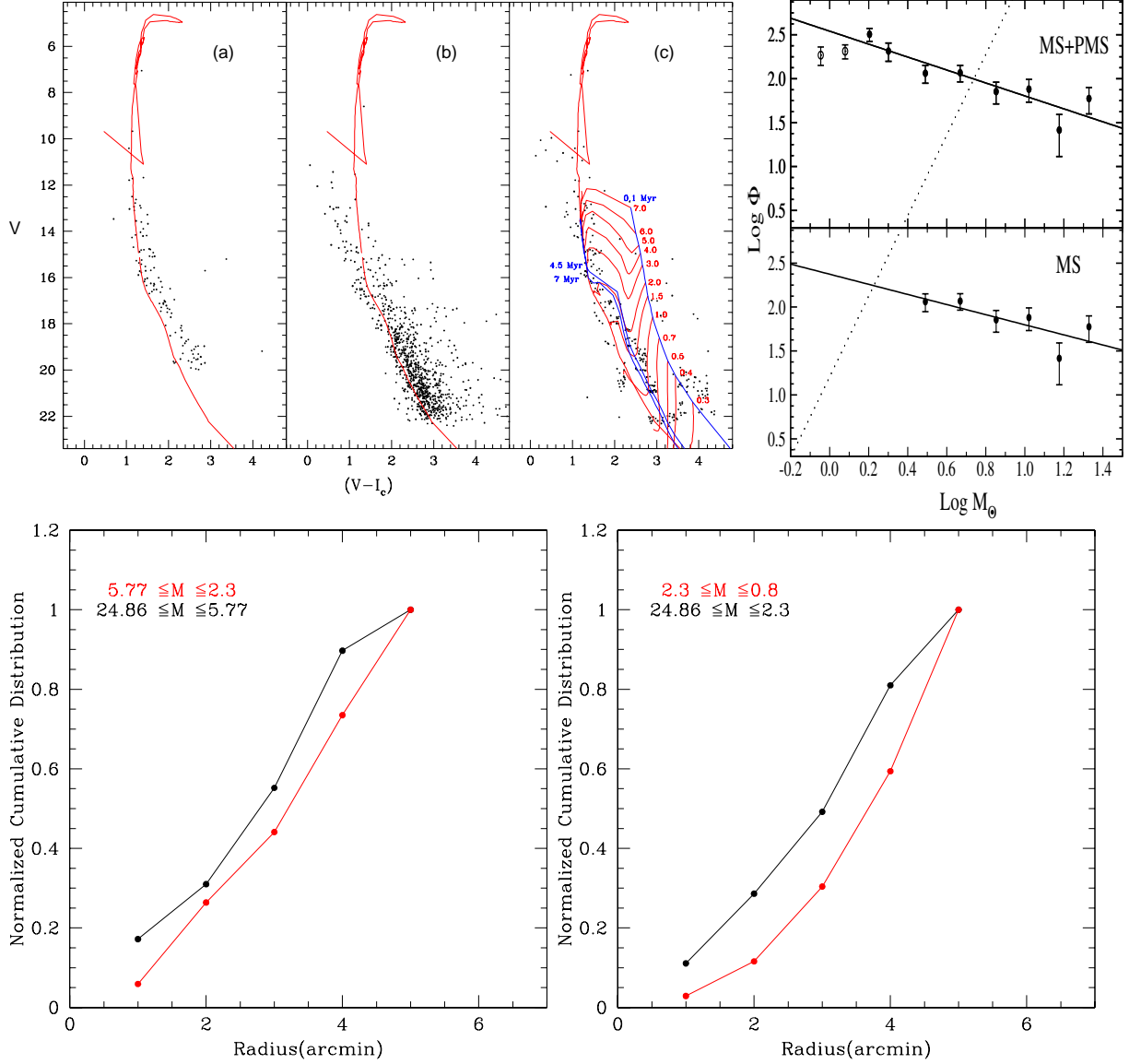


Figure 9. *Top left:* V vs. $(V - I_c)$ CMD for (a) Stars in the NGC 6910 region, (b) Stars in the reference region. and (c) Statistically cleaned CMD overplotted with the isochrone for 4.5 Myr from [Pastorelli et al. \(2019\)](#) (thick red curve) along with the pre-main sequence (PMS) isochrones of 0.1, 4.5 and 7 Myr (blue curves) and the evolutionary tracks of different masses (red curves) from [Siess et al. \(2000\)](#) are shown. All the isochrones and evolutionary tracks are corrected for the distance of 1.72 kpc and reddening $E(B - V) = 0.95$ mag. *Top right:* A plot of MFs for the stars of the NGC 6910. $\log \phi$ represents $\log(dN/d\log m)$. The error bars represent $\pm\sqrt{N}$ error. Continuous curves show a least-squares fit for the given mass range. The upper sub-panel includes stars in the main-sequence (MS) as well as PMS phase whereas the bottom sub-panel includes only MS stars. *Bottom:* Cumulative radial distribution of MS stars (bottom left) and MS+PMS stars (bottom right) for different mass intervals.

the total mass of MS stars ($775 M_\odot$) in the given mass range are obtained with the help of the MF. This total mass of MS stars should be considered as a lower limit to the total mass of the cluster. The half mass radius R_h as half of the cluster radius appears a tenable approximation. We used half of the cluster radius (r_{cl}) obtained from the optical data as the half-mass radius. The dynamical age of this cluster comes out to be 6.5 Myr which is more than the age of this cluster (i.e. 4.5 Myr), suggesting that the dynamics is not fully responsible for the observed mass-segregation and it may be the imprint of star-formation processes itself.

4.2. Physical environment around the cluster

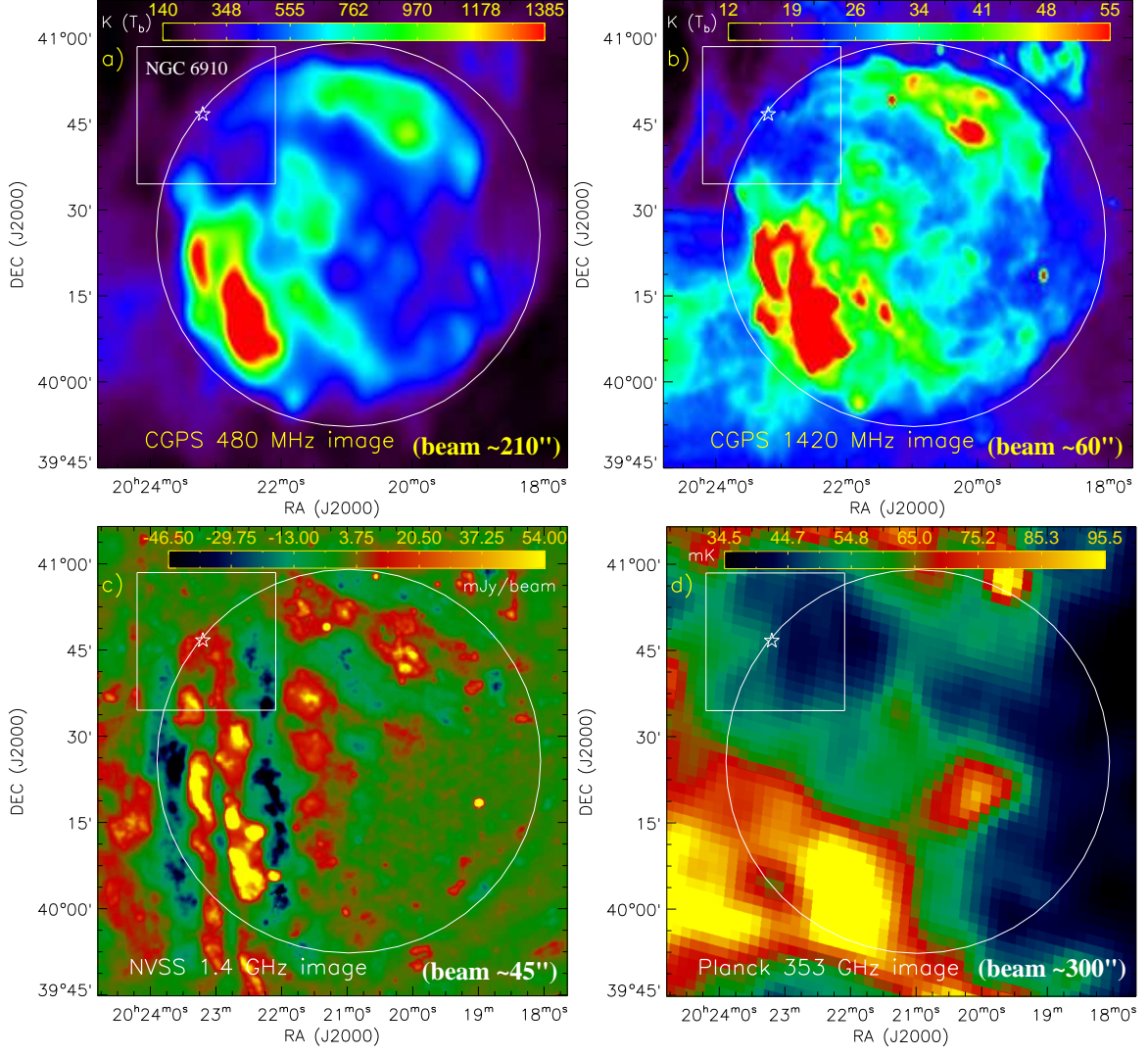


Figure 10. a) CGPS 480 MHz radio continuum image of an area (size $\sim 1^\circ.36 \times 1^\circ.36$; centered at $\alpha_{2000} = 20^h 21^m 15.8^s$, $\delta_{2000} = +40^\circ 25' 49''$) containing the site NGC 6910. b) CGPS 1420 MHz radio continuum image. c) NVSS 1.4 GHz radio continuum image. d) *Planck* 353 GHz continuum image. In each panel, the white box encompasses the area selected in this paper and is shown as a zoomed-in view in Figures 11a and 11b, a circle indicates an extended spherical-like structure traced in the CGPS 1420 MHz continuum image (see Figure 10b) and a star symbol represent the central position of the stellar cluster.

4.2.1. Multi-wavelength picture of the region

Recently available high resolution radio/infrared/sub-millimeter observations have helped us to probe deeply embedded star-forming regions, and have provided a wealth of new information to probe young stars, gas and dust distribution, ionized gas distribution etc, which are very good indicators/tools for star-formation studies (e.g., [Deharveng et al. 2010](#); [Watson et al. 2010](#); [Dewangan et al. 2016, 2017](#)).

In Figures 10a and 10b, the large-scale environment of the cluster NGC 6910 is shown using the CGPS 480 and 1420 MHz continuum images, respectively. These radio continuum images reveal an extended spherical-like structure, which is related to the γ Cygni SNR. Our selected target area is highlighted by a solid box in both the radio continuum images, indicating the location of the NGC 6910 cluster at the border of the SNR. [Uchiyama et al. \(2002\)](#) reported the age of SNR G78.2+2.1 to be 6600 yr. No molecular ^{13}CO emission is observed toward the NGC 6910 cluster (see positions at $l=78.69$ deg; $b=1.96$ deg in Figure 8 in [Piano et al. 2019](#)). It is likely that the SNR might have influenced its surrounding environments. However, the impact of the young SNR G78.2+2.1 on the formation of the relatively old cluster NGC 6910 (~ 4.5 Myr, Section 4.1.4) is unlikely. Figure 10c displays the NVSS 1.4 GHz continuum map. The

NVSS map indicates the presence of the extended diffuse radio continuum emission ($1\sigma \sim 0.45$ mJy/beam) showing existence of radio continuum clumps toward the cluster, which is not seen in the CGPS continuum images having lower sensitivity (see a solid box in Figures 10a, 10b, and 10c). The presence of the radio clumps suggests the existence of embedded massive OB stars, implying the ongoing massive star-formation in the region. Using the *Planck* image at $850 \mu\text{m}$ (or 353 GHz), tracer of the cold dust emission, we show a field hosting the SNR and the cluster NGC 6910 in Figure 10d. It seems that the cluster area is not associated with any noticeable cold dust emission.

Figures 11a and 11b present the *Spitzer* $24 \mu\text{m}$ and *Herschel* $70 \mu\text{m}$ images of the area selected in this paper, respectively. Both the infrared images are overlaid with the NVSS 1.4 GHz continuum emission contours. The extension of the stellar cluster is also marked in both the infrared images. The images at $24 \mu\text{m}$ and $70 \mu\text{m}$ allow to qualitatively trace the warm dust emission present in the cluster NGC 6910. In Figures 11c, 11d, 11e, and 11f, we present a zoomed-in view of the central part of the cluster (see a dashed boxed in Figure 7b) using the $3.6 \mu\text{m}$, $8.0 \mu\text{m}$, $24 \mu\text{m}$, and $70 \mu\text{m}$ images, respectively. These images are also overlaid with the NVSS 1.4 GHz radio continuum emission contours. Diffuse emission is seen in all these infrared images except at $3.6 \mu\text{m}$. We find that the warm dust emission depicted in $24 \mu\text{m}$ and $70 \mu\text{m}$ images is surrounded by the *Spitzer* $8.0 \mu\text{m}$ emission. Note that the *Spitzer* band at $8.0 \mu\text{m}$ hosts PAH features at $7.7 \mu\text{m}$ and $8.6 \mu\text{m}$. Considering the inclusion of PAH features in the $8.0 \mu\text{m}$ band, the existence of PDRs is evident in the NGC 6910 region, suggesting the impact of massive OB stars present in the stellar cluster.

Figure 12a shows the sub-millimeter (sub-mm) image at $350 \mu\text{m}$ (resolution $\sim 25''$), where the extension of the stellar cluster is also marked. In the east direction of the cluster, the sub-mm emission is observed, and is not spatially coincident with the $24 \mu\text{m}$ and $70 \mu\text{m}$ emission (see Figures 11a and 11b). In Figure 12b, we have plotted the stellar surface density contours against the distribution of the warm dust emission and the ionized emission, in the cluster area. In Figure 12b, the warm dust emission is traced using the *Spitzer* $24 \mu\text{m}$ image (see filled area), while the NVSS 1.4 GHz continuum emission depicts the ionized emission (see black contours). We find that the radio continuum peaks (ionized clumps or H II regions) are located away from the center of the cluster (see arrows in Figure 12b). Based on the analysis of the NVSS radio continuum data, we calculate that these ionized clumps are powered by B1V–B0.5V stars (see Table II in Panagia 1973, for a theoretical value), and their dynamical ages are estimated to be ~ 0.07 – 0.12 Myr. In this calculation, we have employed the same procedures as carried out in Dewangan et al. (2017). Using the integrated radio continuum flux density and radius (R_{HII}) of each ionized clump, the number of Lyman continuum photons (N_{uv}) was estimated following the equation given in (Matsakis et al. 1976). Then, with the knowledge of N_{uv} and R_{HII} values, the age of each ionized clump or H II region has been estimated using the equation given in Dyson & Williams (1980).

The *Herschel* temperature and column density maps can be used to deduce the physical conditions present in a given star-forming region (cf. Dewangan 2019; Dewangan et al. 2019a,b). Figures 12c and 12d show the *Herschel* temperature and column density maps (resolution $\sim 12''$), respectively. These *Herschel* maps are also overlaid with the NVSS radio continuum emission contours. In Figure 12c, we have traced a feature in the temperature map using a contour of $T_d = 17.5$ K (\approx average dust temperature). Using a black broken contour, this feature is also highlighted in both the *Herschel* maps. The ionized clumps distributed within the cluster are associated with emission at $T_d = 17.5$ – 18.0 K. In Figure 12d, we do not find high column density materials in the direction of the cluster except in the east direction where radio peaks are seen harboring the very young stellar sources.

4.2.2. The star formation scenario

Our careful analysis of various observational data sets suggests that the MF slope of the cluster region is shallower than the Salpeter value (i.e., $\Gamma = -1.35$). It shows a signature of the presence of more massive stars compared to the low mass stars in the cluster region. This argument suggests the effect of mass-segregation. A comparison between the cluster age (i.e., ~ 4.5 Myr) and its dynamical relaxation time (i.e. ~ 6.5 Myr) indicates that the cluster is not relaxed yet. Furthermore, the observed mass-segregation seen in this cluster may be the imprint of their formation processes. These properties make the NGC 6910 cluster a special target to study the feedback effect of massive star(s) on its environment.

Massive stars can provide positive feedback affecting star-formation by accumulating neutral material at the periphery of H II regions via ‘collect and collapse’ mechanism (Elmegreen & Lada 1977; Whitworth et al. 1994), or by the compression of pre-existing dense condensations via ‘radiation-driven implosion’ mechanism (RDI; Bertoldi 1989; Lefloch & Lazareff 1994). Star-formation induced in a region by these processes is also called triggered-star-formation

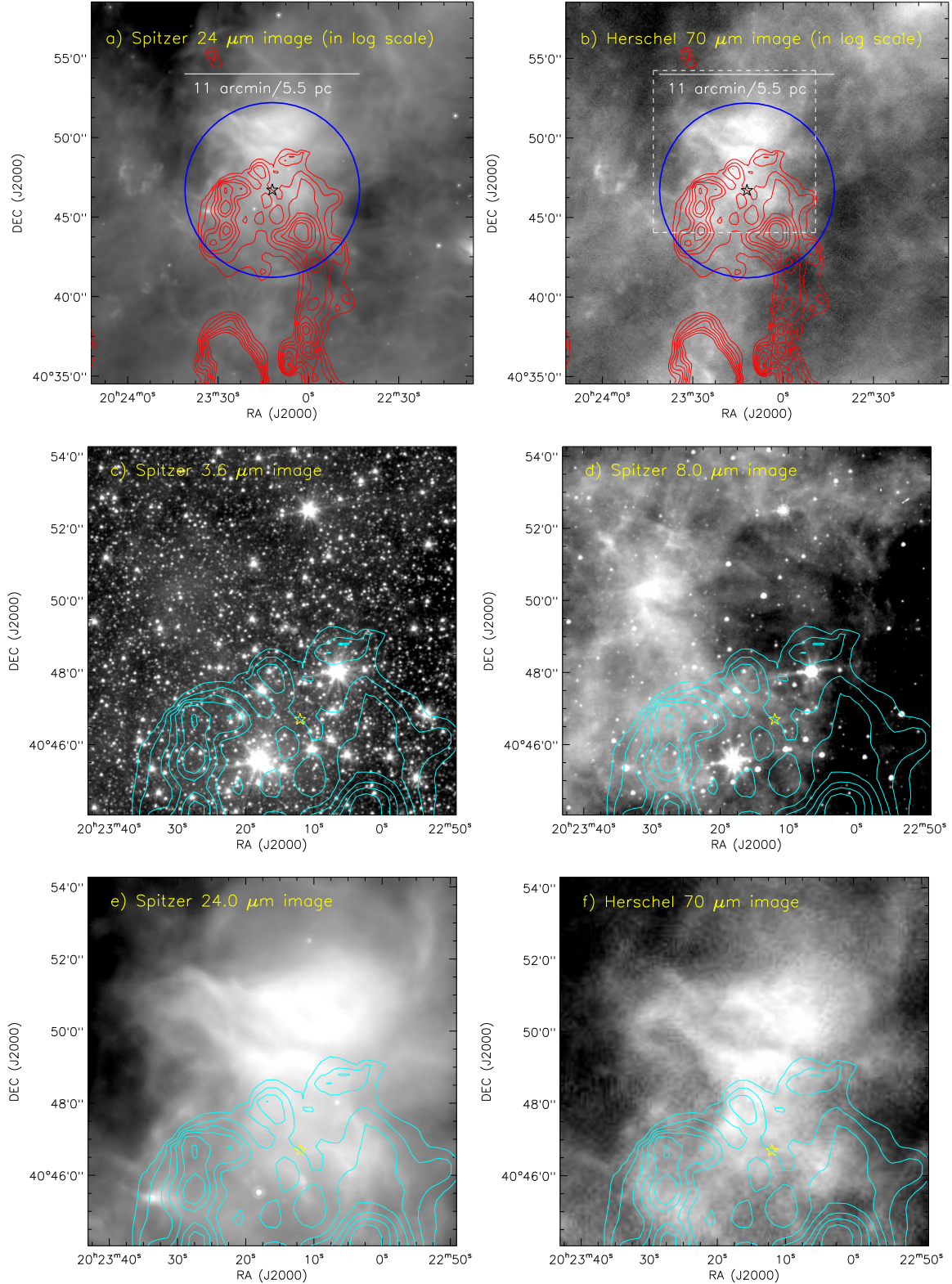


Figure 11. a) The panel shows the *Spitzer* image at 24 μm overlaid with the NVSS radio continuum contours (in red) at 1.4 GHz (see a solid box in Figure 10a). b) Overlay of the 1.4 GHz NVSS radio continuum contours (in red) on the *Herschel* image at 70 μm . The white box is shown as a zoomed-in view in Figures 11c, 11d, 11e, and 11f. c) The panel displays the *Spitzer* image at 3.6 μm superimposed with the NVSS radio continuum contours (in cyan) at 1.4 GHz (see a white box in Figure 11b). d) Overlay of the NVSS radio continuum contours (in cyan) at 1.4 GHz on the *Spitzer* image at 8.0 μm . e) The panel presents the *Spitzer* image at 24 μm overlaid with the NVSS 1.4 GHz continuum contours (in cyan) at 1.4 GHz. f) Overlay of the NVSS 1.4 GHz continuum contours (in cyan) on the *Herschel* image at 70 μm . In the panels (a) and (b), an extension of the stellar cluster is indicated by a big circle. In all the panels, a star symbol represents the central position of the stellar cluster. The NVSS contours are shown with the levels of 6, 8, 10, 12, 15, 18, and 22 mJy/beam, where $1\sigma \sim 0.45$ mJy/beam.

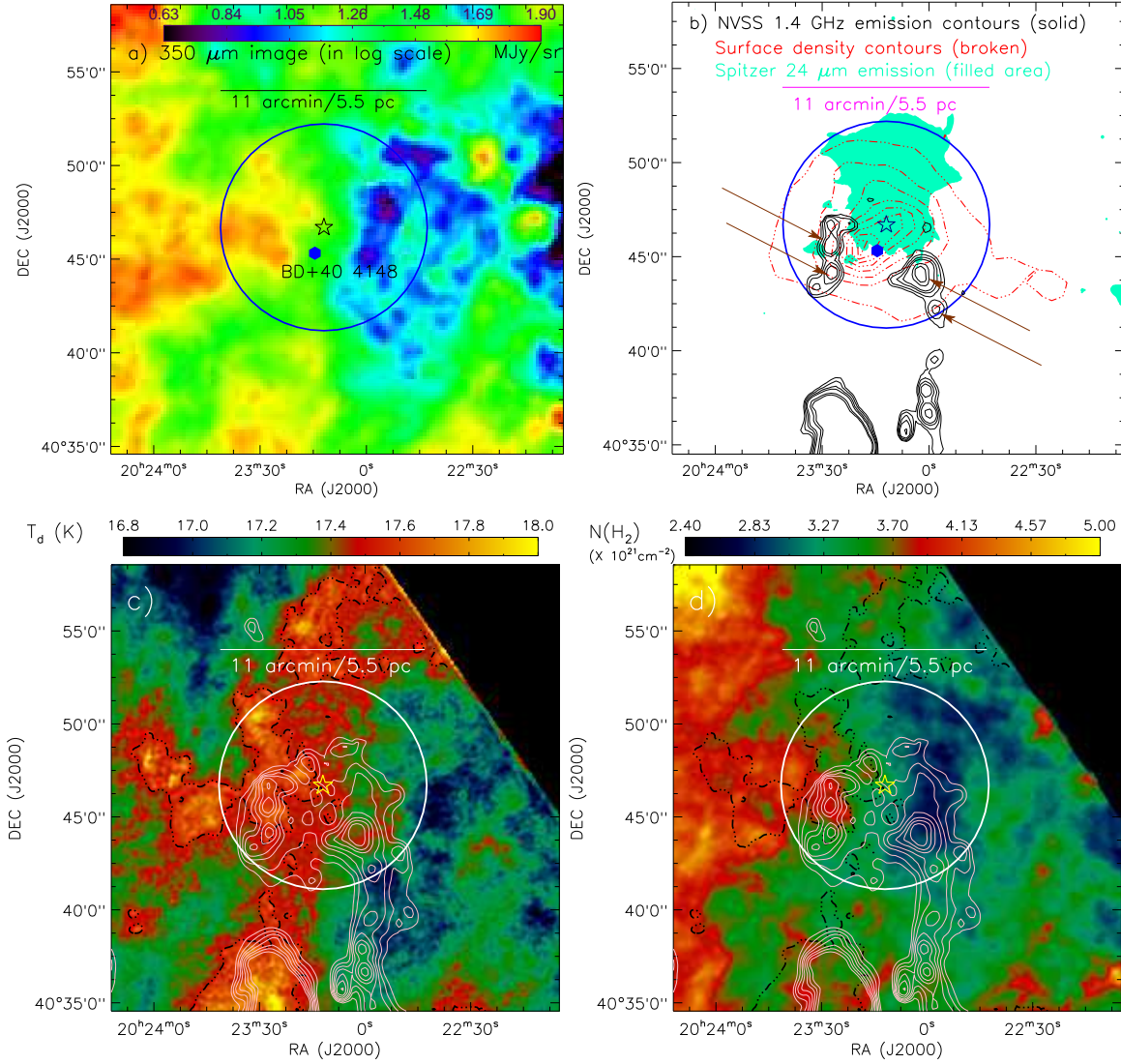


Figure 12. a) *Herschel* image at $350\ \mu\text{m}$ (see a solid box in Figure 10a). A filled hexagon indicates the position of a massive star BD+40 4148 (spectral class = O9.5V; Hoag & Applequist 1965). b) Overlay of the stellar surface density contours (in red) and the radio continuum emission contours (in black) on the feature traced in the *Spitzer* $24\ \mu\text{m}$ image (i.e., filled area). The NVSS contours (in black) are shown with the levels of 11.5, 13, 15, 17, 22, and 25 mJy/beam, where $1\sigma \sim 0.45$ mJy/beam. A filled area traced in the *Spitzer* $24\ \mu\text{m}$ image is shown with a contour of 58 MJy/sr. The lowest stellar surface density contour (in red) is 1σ (i.e., 2.2 stars/pc² at 1720 pc), and the step size is equal to 1σ . Arrows highlight the NVSS radio peaks observed toward the cluster. c) Overlay of the 1.4 GHz NVSS radio continuum contours (in pink) on the *Herschel* temperature map. d) Overlay of the 1.4 GHz NVSS radio continuum contours (in pink) on the *Herschel* column density ($N(\text{H}_2)$) map. In the panels (c) and (d), the radio emission contours are as same as in Figure 11a, and the broken contour (in black) indicates the dust temperature (T_d) at 17.5 K. In all the panels, a star symbol represents the central position of the stellar cluster, and an extension of the cluster is indicated by a big circle.

and observational signposts usually include age sequence of the stellar sources and the distribution of cool, warm and ionized gas in the region (see also, Samal et al. 2007; Jose et al. 2011; Sharma et al. 2007, 2012, 2017). Observational studies of bubbles associated with H II regions created by massive stars suggest that their expansion probably triggers 14% to 30% of star-formation in our Galaxy (e.g., Deharveng et al. 2010; Thompson et al. 2012; Kendrew et al. 2012), thus implying the importance of massive OB stars on the star-formation activities in our Galaxy.

The cluster NGC 6910 contains several massive OB stars and the most massive of them is an O9.5V star known as BD+40 4148 (Hoag & Applequist 1965). The position of this massive star is marked by a diamond in Figure 2. In general, a massive star can influence the surroundings through its different feedback pressure components (such as, pressure

of an H II region (P_{HII}), radiation pressure (P_{rad}), and stellar wind ram pressure (P_{wind}) (see e.g., Bressert et al. 2012; Dewangan et al. 2017). These pressure components can be expressed as below (see e.g., Bressert et al. 2012):

$$P_{HII} = \mu m_H c_s^2 \left(\sqrt{\frac{3N_{uv}}{4\pi\alpha_B D_s^3}} \right); \quad (10)$$

$$P_{rad} = L_{bol}/4\pi c D_s^2; \quad (11)$$

$$P_{wind} = \dot{M}_w V_w / 4\pi D_s^2; \quad (12)$$

In the equations above, ' N_{uv} ' is the Lyman continuum photons, ' c_s ' is the sound speed in the photoionized region ($= 11 \text{ km s}^{-1}$; Bisbas et al. 2009), ' α_B ' is the radiative recombination coefficient ($= 2.6 \times 10^{-13} \times (10^4 \text{ K}/T_e)^{0.7} \text{ cm}^3 \text{ s}^{-1}$; Kwan 1997), ' μ ' is the mean molecular weight in the ionized gas ($= 0.678$; Bisbas et al. 2009), ' m_H ' is the hydrogen atom mass, ' \dot{M}_w ' is the mass-loss rate, ' V_w ' is the wind velocity of the ionizing source, and ' L_{bol} ' is the bolometric luminosity of the ionizing source. ' D_s ' is the projected distance from the location of the O9.5V type star to the ionized clumps, which is adopted to be 1.0 pc (see Figure 12b).

We have used $L_{bol} = 66070 L_\odot$ (Panagia 1973), $\dot{M}_w \approx 1.58 \times 10^{-9} M_\odot \text{ yr}^{-1}$ (Marcolino et al. 2009), $V_w \approx 1500 \text{ km s}^{-1}$ (Marcolino et al. 2009), and $N_{uv} = 1.2 \times 10^{48} \text{ phs}^{-1}$ (Panagia 1973) for a star of O9.5V spectral type to estimate different pressure components which comes out to be $P_{HII} \approx 2.6 \times 10^{-10} \text{ dynes cm}^{-2}$, $P_{rad} \approx 7.1 \times 10^{-11} \text{ dynes cm}^{-2}$, and $P_{wind} \approx 1.3 \times 10^{-13} \text{ dynes cm}^{-2}$. It gives a total pressure (i.e., $P_{total} = P_{HII} + P_{rad} + P_{wind}$) driven by a massive star as $\sim 3.4 \times 10^{-10} \text{ dynes cm}^{-2}$. It appears that the P_{HII} component is relatively higher than other two pressure components. Furthermore, we find that the value of P_{total} is also higher than the pressure of a typical cool molecular cloud ($P_{MC} \sim 10^{-11} - 10^{-12} \text{ dynes cm}^{-2}$ for a temperature $\sim 20 \text{ K}$ and particle density $\sim 10^3 - 10^4 \text{ cm}^{-3}$) (see Table 7.3 of Dyson & Williams 1980). It suggests that the massive star seems to have significantly influenced its environment. Additionally, the photoionized gas associated with the cluster appears to be responsible for the feedback mechanism.

We also find the existence of young ionized clumps, located along the edge of the NGC 6910 cluster containing massive stars, in a high column density region. The center of the cluster is associated with warm dust emission, and the ionized clumps are distributed in the PDRs. Hence, it is likely that these massive stars might have influenced the birth of the youngest massive B-type stars (age range $\sim 0.07 - 0.12 \text{ Myr}$) powering the ionized clumps. In a triggered star-forming region 'Sh 2-294', Samal et al. (2007) have also found ionized clumps away from the exciting source. We did not find any ring/arc of gas and dust surrounding the NGC 6910 cluster as has been found in the regions showing collect and collapse mechanism (for details, cf. Deharveng et al. 2005). Therefore, the age difference between the young sources in region and the central massive source, and the distribution of PDRs/warm and cold gas and dust/ionized gas, seem to be consistent with the hypothesis that the star-formation at the border of NGC 6910 may be due to the RDI process. However, with the currently available observations and data, it will be early to establish or rule out either of the scenarios.

5. SUMMARY AND CONCLUSIONS

We have performed deep multiband ($UBV(RI)_c$) and wide-field optical photometric observations ($FOV \sim 22 \times 23 \text{ arcmin}^2$) around the NGC 6910 cluster up to 22 mag in the V-band. The data is complete down to 20.6 mag in the V-band, corresponding to the mass completeness of $0.8 M_\odot$. The optical data along with multiwavelength archival data have been used to study the ongoing physical processes in the cluster NGC 6910. The main results are summarized below:

- By using the radial density profile of stellar sources, we estimated the cluster radius as 5.5 arcmin with a core radius of 1.4 arcmin. We have used the stellar surface density contours to study the structure of this cluster and found that the stellar surface density contours match with the cluster size determined by the RDP. The core region of this cluster seems to be elongated.
- We have calculated the membership probability for 916 stars in the cluster NGC 6910 and found 128 member stars with membership probabilities higher than 80% with $G < 20 \text{ mag}$. We have calculated a distance to the cluster as $1.72 \pm 0.08 \text{ kpc}$ using parallax for cluster members. With the help of TCDs and CMDs, we have also

estimated the foreground reddening $E(B - V)_{min}$, distance, and age of the cluster NGC 6910 to be 0.95 mag, 1.72 kpc, and 4.5 Myr, respectively.

- It is found that the mass function slope ‘T’ in the cluster region (i.e. -0.74 ± 0.15) is shallower than the Salpeter value (i.e., -1.35), which indicates the presence of large number of massive stars as compared to low mass stars in the cluster region and indicates an effect of mass-segregation. A contrast between cluster age (i.e., ~ 4.5 Myr) and its dynamical relaxation time (i.e. ~ 6.5 Myr) suggests that the cluster is not relaxed yet, and the observed mass-segregation seen in this cluster may be the imprint of their formation processes.
- The distribution of warm dust is found in the central region of the cluster which also contain massive stars. The cluster is surrounded by the PDRs along with the presence of radio peaks (ionized clumps) and cold gas. The total pressure (i.e. $P_{total} \sim 3.4 \times 10^{-10}$ dynes cm^{-2}) driven by the massive O9.5V star (BD+40 4148) at the location of the ionized clumps is also found to be very high as compared to the pressure of a typical cool molecular cloud. All these signatures strongly suggest the influence of massive star(s) of the NGC 6910 cluster on its environment.
- We have determined the spectral type and age of the young star responsible for the radio emission near the border of the cluster (ionized clumps) as B-type and ~ 0.07 – 0.12 Myr, respectively. The age gradient between the central massive star (4.5 Myr) and the ionized clumps (~ 0.07 – 0.12 Myr) along with other signatures indicates the influence of massive star(s). This suggests that the feedback effects from the central massive stars are triggering the formation of next generation of stars in the surrounding region.

ACKNOWLEDGMENTS

We thank the anonymous reviewer for a critical reading of the manuscript and constructive suggestions, which greatly improved the overall quality of the paper. The observations reported in this paper were obtained using the 1-m Sampurnanand Telescope, Nainital, India. This work is based on data obtained as part of the UKIRT Infrared Deep Sky Survey (UKIDSS). This publication made use of data products from the 2MASS (a joint project of the University of Massachusetts and the Infrared Processing and Analysis Center/California Institute of Technology, funded by NASA and NSF), archival data obtained with the Spitzer Space Telescope (operated by the Jet Propulsion Laboratory, California Institute of Technology under a contract with NASA). This study has made use of data from the European Space Agency (ESA) mission *Gaia* (<https://www.cosmos.esa.int/gaia>), processed by the *Gaia* Data Processing and Analysis Consortium (DPAC; <https://www.cosmos.esa.int/web/gaia/dpac/consortium>). Funding for the DPAC has been provided by the institutions participating in the *Gaia* Multilateral Agreement. DKO acknowledges the support of the Department of Atomic Energy, Government of India, under project No. 12-R&D-TFR-5.02-0200. LKD acknowledges the support of the Department of Space, Government of India.

Software: ESO-MIDAS (Banse et al. 1992), IRAF (Tody 1986, 1993), DAOPHOT-II software (Stetson 1987)

REFERENCES

- Adelman, S. J., & Yüce, K. 2007, *Baltic Astronomy*, 16, 311
- Appenzeller, I., & Wendker, H. J. 1980, *A&A*, 89, 239
- Arhipova, V. P., & Lozinskaia, T. A. 1978, *AZh*, 55, 1320
- Baars, J. W. M., & Wendker, H. J. 1981, *A&A*, 101, 39
- Bailer-Jones, C. A. L., Rybizki, J., Fousneau, M., Mantelet, G., & Andrae, R. 2018, *AJ*, 156, 58, doi: [10.3847/1538-3881/aacb21](https://doi.org/10.3847/1538-3881/aacb21)
- Balaguer-Núñez, L., Tian, K. P., & Zhao, J. L. 1998, *A&AS*, 133, 387, doi: [10.1051/aas:1998324](https://doi.org/10.1051/aas:1998324)
- Banse, K., Grosbol, P., & Baade, D. 1992, *Astronomical Society of the Pacific Conference Series*, Vol. 25, MIDAS as a Development Environment, ed. D. M. Worrall, C. Biemesderfer, & J. Barnes, 120
- Bastian, N., Covey, K. R., & Meyer, M. R. 2010, *ARA&A*, 48, 339, doi: [10.1146/annurev-astro-082708-101642](https://doi.org/10.1146/annurev-astro-082708-101642)
- Battinelli, P., & Capuzzo-Dolcetta, R. 1991, *MNRAS*, 249, 76, doi: [10.1093/mnras/249.1.76](https://doi.org/10.1093/mnras/249.1.76)
- Becker, W., & Fenkart, R. 1971, *A&AS*, 4, 241
- Bellini, A., Piotto, G., Bedin, L. R., et al. 2009, *A&A*, 493, 959, doi: [10.1051/0004-6361:200810880](https://doi.org/10.1051/0004-6361:200810880)
- Bertoldi, F. 1989, *ApJ*, 346, 735, doi: [10.1086/168055](https://doi.org/10.1086/168055)
- Bisbas, T. G., Wunsch, R., Whitworth, A. P., & Hubber, D. A. 2009, *A&A*, 497, 649, doi: [10.1051/0004-6361/200811522](https://doi.org/10.1051/0004-6361/200811522)
- Bonnell, I. A., Bate, M. R., & Zinnecker, H. 1998, *MNRAS*, 298, 93, doi: [10.1046/j.1365-8711.1998.01590.x](https://doi.org/10.1046/j.1365-8711.1998.01590.x)

- Bossini, D., Vallenari, A., Bragaglia, A., et al. 2019, *A&A*, 623, A108, doi: [10.1051/0004-6361/201834693](https://doi.org/10.1051/0004-6361/201834693)
- Bressert, E., Ginsburg, A., Bally, J., et al. 2012, *ApJL*, 758, L28, doi: [10.1088/2041-8205/758/2/L28](https://doi.org/10.1088/2041-8205/758/2/L28)
- Cardelli, J. A., Clayton, G. C., & Mathis, J. S. 1989, *ApJ*, 345, 245, doi: [10.1086/167900](https://doi.org/10.1086/167900)
- Carey, S. J., Noriega-Crespo, A., Price, S. D., et al. 2005, in *American Astronomical Society Meeting Abstracts*, Vol. 207, 63.33
- Chabrier, G. 2003, *PASP*, 115, 763, doi: [10.1086/376392](https://doi.org/10.1086/376392)
- Chauhan, N., Pandey, A. K., Ogura, K., et al. 2011, *MNRAS*, 415, 1202, doi: [10.1111/j.1365-2966.2011.18742.x](https://doi.org/10.1111/j.1365-2966.2011.18742.x)
- Chen, W. P., Chen, C. W., & Shu, C. G. 2004, *AJ*, 128, 2306, doi: [10.1086/424855](https://doi.org/10.1086/424855)
- Chini, R., Kruegel, E., & Kreysa, E. 1990, *A&A*, 227, L5
- Comerón, F., & Pasquali, A. 2012, *A&A*, 543, A101, doi: [10.1051/0004-6361/201219022](https://doi.org/10.1051/0004-6361/201219022)
- Condon, J. J., Cotton, W. D., Greisen, E. W., et al. 1998, *AJ*, 115, 1693, doi: [10.1086/300337](https://doi.org/10.1086/300337)
- Corbelli, E., Palla, F., & Zinnecker, H., eds. 2005, *Astrophysics and Space Science Library*, Vol. 327, The Initial Mass Function 50 years later
- Dambis, A. K. 1999, *Astronomy Letters*, 25, 7
- Dame, T. M., Hartmann, D., & Thaddeus, P. 2001, *ApJ*, 547, 792, doi: [10.1086/318388](https://doi.org/10.1086/318388)
- Davies, R. D., & Tovmassian, H. M. 1963, *MNRAS*, 127, 45, doi: [10.1093/mnras/127.1.45](https://doi.org/10.1093/mnras/127.1.45)
- Deharveng, L., Zavagno, A., & Caplan, J. 2005, *A&A*, 433, 565, doi: [10.1051/0004-6361:20041946](https://doi.org/10.1051/0004-6361:20041946)
- Deharveng, L., Schuller, F., Anderson, L. D., et al. 2010, *A&A*, 523, A6, doi: [10.1051/0004-6361/201014422](https://doi.org/10.1051/0004-6361/201014422)
- Deharveng, L., Zavagno, A., Samal, M. R., et al. 2015, *A&A*, 582, A1, doi: [10.1051/0004-6361/201423835](https://doi.org/10.1051/0004-6361/201423835)
- Delgado, A. J., & Alfaro, E. J. 2000, *AJ*, 119, 1848, doi: [10.1086/301298](https://doi.org/10.1086/301298)
- Dewangan, L. K. 2019, *ApJ*, 884, 84, doi: [10.3847/1538-4357/ab4189](https://doi.org/10.3847/1538-4357/ab4189)
- Dewangan, L. K., Ojha, D. K., Luna, A., et al. 2016, *ApJ*, 819, 66, doi: [10.3847/0004-637X/819/1/66](https://doi.org/10.3847/0004-637X/819/1/66)
- Dewangan, L. K., Ojha, D. K., Zinchenko, I., Janardhan, P., & Luna, A. 2017, *ApJ*, 834, 22, doi: [10.3847/1538-4357/834/1/22](https://doi.org/10.3847/1538-4357/834/1/22)
- Dewangan, L. K., Pirogov, L. E., Ryabukhina, O. L., Ojha, D. K., & Zinchenko, I. 2019a, *ApJ*, 877, 1, doi: [10.3847/1538-4357/ab1aa6](https://doi.org/10.3847/1538-4357/ab1aa6)
- Dewangan, L. K., Sano, H., Enokiya, R., et al. 2019b, *ApJ*, 878, 26, doi: [10.3847/1538-4357/ab1cba](https://doi.org/10.3847/1538-4357/ab1cba)
- Dickel, H. R., Seacord, II, A. W., & Gottesman, S. T. 1977, *ApJ*, 218, 133, doi: [10.1086/155665](https://doi.org/10.1086/155665)
- Dyson, J. E., & Williams, D. A. 1980, *Physics of the interstellar medium*
- Elmegreen, B. G., & Lada, C. J. 1977, *ApJ*, 214, 725, doi: [10.1086/155302](https://doi.org/10.1086/155302)
- Friel, E. D., Donati, P., Bragaglia, A., et al. 2014, *A&A*, 563, A117, doi: [10.1051/0004-6361/201323215](https://doi.org/10.1051/0004-6361/201323215)
- Gaia Collaboration, Katz, D., Antoja, T., et al. 2018a, *A&A*, 616, A11, doi: [10.1051/0004-6361/201832865](https://doi.org/10.1051/0004-6361/201832865)
- Gaia Collaboration, Brown, A. G. A., Vallenari, A., et al. 2018b, *A&A*, 616, A1, doi: [10.1051/0004-6361/201833051](https://doi.org/10.1051/0004-6361/201833051)
- Girard, T. M., Grundy, W. M., Lopez, C. E., & van Altena, W. F. 1989, *AJ*, 98, 227, doi: [10.1086/115139](https://doi.org/10.1086/115139)
- Golay, M., ed. 1974, *Astrophysics and Space Science Library*, Vol. 41, Introduction to astronomical photometry
- Guetter, H. H., & Vrba, F. J. 1989, *AJ*, 98, 611, doi: [10.1086/115161](https://doi.org/10.1086/115161)
- Gutermuth, R. A., Megeath, S. T., Pipher, J. L., et al. 2005, *ApJ*, 632, 397, doi: [10.1086/432460](https://doi.org/10.1086/432460)
- Harris, G. L. H. 1976, *ApJS*, 30, 451, doi: [10.1086/190368](https://doi.org/10.1086/190368)
- Hoag, A. A., & Applequist, N. L. 1965, *ApJS*, 12, 215, doi: [10.1086/190125](https://doi.org/10.1086/190125)
- Humphreys, R. M. 1978, *ApJS*, 38, 309, doi: [10.1086/190559](https://doi.org/10.1086/190559)
- Hur, H., Sung, H., & Bessell, M. S. 2012, *AJ*, 143, 41, doi: [10.1088/0004-6256/143/2/41](https://doi.org/10.1088/0004-6256/143/2/41)
- Jose, J., Herczeg, G. J., Samal, M. R., Fang, Q., & Panwar, N. 2017, *ApJ*, 836, 98, doi: [10.3847/1538-4357/836/1/98](https://doi.org/10.3847/1538-4357/836/1/98)
- Jose, J., Pandey, A. K., Ogura, K., et al. 2011, *MNRAS*, 411, 2530, doi: [10.1111/j.1365-2966.2010.17860.x](https://doi.org/10.1111/j.1365-2966.2010.17860.x)
- Jose, J., Pandey, A. K., Samal, M. R., et al. 2013, *MNRAS*, 432, 3445, doi: [10.1093/mnras/stt700](https://doi.org/10.1093/mnras/stt700)
- Kaluzny, J., & Udalski, A. 1992, *AcA*, 42, 29
- Kendrew, S., Simpson, R., Bressert, E., et al. 2012, *ApJ*, 755, 71, doi: [10.1088/0004-637X/755/1/71](https://doi.org/10.1088/0004-637X/755/1/71)
- King, I. 1962, *AJ*, 67, 471, doi: [10.1086/108756](https://doi.org/10.1086/108756)
- Kolaczowski, Z., Pigulski, A., Kopacki, G., & Michalska, G. 2004, *AcA*, 54, 33
- Kroupa, P. 2002, *Science*, 295, 82, doi: [10.1126/science.1067524](https://doi.org/10.1126/science.1067524)
- Kubát, J., Korčáková, D., Kawka, A., et al. 2007, *A&A*, 472, 163, doi: [10.1051/0004-6361:20077171](https://doi.org/10.1051/0004-6361:20077171)
- Kumar, B., Sharma, S., Manfroid, J., et al. 2014, *A&A*, 567, A109, doi: [10.1051/0004-6361/201323027](https://doi.org/10.1051/0004-6361/201323027)
- Kwan, J. 1997, *ApJ*, 489, 284, doi: [10.1086/304773](https://doi.org/10.1086/304773)
- Landecker, T. L., Roger, R. S., & Higgs, L. A. 1980, *A&AS*, 39, 133
- Landolt, A. U. 1992, *AJ*, 104, 340, doi: [10.1086/116242](https://doi.org/10.1086/116242)

- Lawrence, A., Warren, S. J., Almaini, O., et al. 2007, *MNRAS*, 379, 1599, doi: [10.1111/j.1365-2966.2007.12040.x](https://doi.org/10.1111/j.1365-2966.2007.12040.x)
- Lefloch, B., & Lazareff, B. 1994, *A&A*, 289, 559
- Lim, B., Sung, H. S., Karimov, R., & Ibrahimov, M. 2011, *Journal of Korean Astronomical Society*, 44, 39. <https://arxiv.org/abs/1103.4927>
- Marcolino, W. L. F., Bouret, J. C., Martins, F., et al. 2009, *A&A*, 498, 837, doi: [10.1051/0004-6361/200811289](https://doi.org/10.1051/0004-6361/200811289)
- Marsh, K. A., Whitworth, A. P., & Lomax, O. 2015, *MNRAS*, 454, 4282, doi: [10.1093/mnras/stv2248](https://doi.org/10.1093/mnras/stv2248)
- Marsh, K. A., Whitworth, A. P., Lomax, O., et al. 2017, *MNRAS*, 471, 2730, doi: [10.1093/mnras/stx1723](https://doi.org/10.1093/mnras/stx1723)
- Massey, P., & Thompson, A. B. 1991, *AJ*, 101, 1408, doi: [10.1086/115774](https://doi.org/10.1086/115774)
- Mathieu, R. D. 1985, in *IAU Symposium*, Vol. 113, *Dynamics of Star Clusters*, ed. J. Goodman & P. Hut, 427–446
- Matsakis, D. N., Evans, N. J., I., Sato, T., & Zuckerman, B. 1976, *AJ*, 81, 172, doi: [10.1086/111871](https://doi.org/10.1086/111871)
- McNamara, B. J., & Sekiguchi, K. 1986, *ApJ*, 310, 613, doi: [10.1086/164714](https://doi.org/10.1086/164714)
- Melikian, N. D., & Shevchenko, V. S. 1990, *Astrofizika*, 32, 169
- Mermilliod, J.-C. 2000, in *Astronomical Society of the Pacific Conference Series*, Vol. 211, *Massive Stellar Clusters*, ed. A. Lançon & C. M. Boily, 43
- Molinari, S., Swinyard, B., Bally, J., et al. 2010, *PASP*, 122, 314, doi: [10.1086/651314](https://doi.org/10.1086/651314)
- Panagia, N. 1973, *AJ*, 78, 929, doi: [10.1086/111498](https://doi.org/10.1086/111498)
- Pandey, A. K., Nilakshi, Ogura, K., Sagar, R., & Tarusawa, K. 2001, *A&A*, 374, 504, doi: [10.1051/0004-6361:20010642](https://doi.org/10.1051/0004-6361:20010642)
- Pandey, A. K., Ogura, K., & Sekiguchi, K. 2000, *PASJ*, 52, 847, doi: [10.1093/pasj/52.5.847](https://doi.org/10.1093/pasj/52.5.847)
- Pandey, A. K., Sharma, S., Kobayashi, N., Sarugaku, Y., & Ogura, K. 2020a, *MNRAS*, 492, 2446, doi: [10.1093/mnras/stz3596](https://doi.org/10.1093/mnras/stz3596)
- Pandey, A. K., Sharma, S., Ogura, K., et al. 2008, *MNRAS*, 383, 1241, doi: [10.1111/j.1365-2966.2007.12641.x](https://doi.org/10.1111/j.1365-2966.2007.12641.x)
- Pandey, A. K., Upadhyay, K., Nakada, Y., & Ogura, K. 2003, *A&A*, 397, 191, doi: [10.1051/0004-6361:20021509](https://doi.org/10.1051/0004-6361:20021509)
- Pandey, A. K., Upadhyay, K., Ogura, K., et al. 2005, *MNRAS*, 358, 1290, doi: [10.1111/j.1365-2966.2005.08784.x](https://doi.org/10.1111/j.1365-2966.2005.08784.x)
- Pandey, A. K., Eswaraiah, C., Sharma, S., et al. 2013, *ApJ*, 764, 172, doi: [10.1088/0004-637X/764/2/172](https://doi.org/10.1088/0004-637X/764/2/172)
- Pandey, R., Sharma, S., Panwar, N., et al. 2020b, *ApJ*, 891, 81, doi: [10.3847/1538-4357/ab6dc7](https://doi.org/10.3847/1538-4357/ab6dc7)
- Panwar, N., Pandey, A. K., Samal, M. R., et al. 2018, *AJ*, 155, 44, doi: [10.3847/1538-3881/aa9f1b](https://doi.org/10.3847/1538-3881/aa9f1b)
- Pastorelli, G., Marigo, P., Girardi, L., et al. 2019, *MNRAS*, 485, 5666, doi: [10.1093/mnras/stz725](https://doi.org/10.1093/mnras/stz725)
- Pecaut, M. J., & Mamajek, E. E. 2013, *ApJS*, 208, 9, doi: [10.1088/0067-0049/208/1/9](https://doi.org/10.1088/0067-0049/208/1/9)
- Perren, G. I., Vázquez, R. A., & Piatti, A. E. 2015, *A&A*, 576, A6, doi: [10.1051/0004-6361/201424946](https://doi.org/10.1051/0004-6361/201424946)
- Phelps, R. L., & Janes, K. A. 1994, *ApJS*, 90, 31, doi: [10.1086/191857](https://doi.org/10.1086/191857)
- Piano, G., Cardillo, M., Pilia, M., et al. 2019, *ApJ*, 878, 54, doi: [10.3847/1538-4357/ab1f69](https://doi.org/10.3847/1538-4357/ab1f69)
- Planck Collaboration, Ade, P. A. R., Aghanim, N., et al. 2014, *A&A*, 571, A9, doi: [10.1051/0004-6361/201321531](https://doi.org/10.1051/0004-6361/201321531)
- Reddish, V. C., Lawrence, L. C., & Pratt, N. M. 1966, *Publications of the Royal Observatory of Edinburgh*, 5, 111
- Reipurth, B., & Schneider, N. 2008, *Star Formation and Young Clusters in Cygnus*, ed. B. Reipurth, 36
- Sagar, R., & Richtler, T. 1991, *A&A*, 250, 324
- Salpeter, E. E. 1955, *ApJ*, 121, 161, doi: [10.1086/145971](https://doi.org/10.1086/145971)
- Samal, M. R., Pandey, A. K., Ojha, D. K., et al. 2007, *ApJ*, 671, 555, doi: [10.1086/522941](https://doi.org/10.1086/522941)
- Sandell, G., Wiesemeyer, H., Requena-Torres, M. A., et al. 2012, *A&A*, 542, L14, doi: [10.1051/0004-6361/201218920](https://doi.org/10.1051/0004-6361/201218920)
- Sariya, D. P., Jiang, I.-G., & Yadav, R. K. S. 2017, *AJ*, 153, 134, doi: [10.3847/1538-3881/aa5be6](https://doi.org/10.3847/1538-3881/aa5be6)
- Sariya, D. P., & Yadav, R. K. S. 2015, *A&A*, 584, A59, doi: [10.1051/0004-6361/201526688](https://doi.org/10.1051/0004-6361/201526688)
- Sariya, D. P., Yadav, R. K. S., & Bellini, A. 2012, *A&A*, 543, A87, doi: [10.1051/0004-6361/201219306](https://doi.org/10.1051/0004-6361/201219306)
- Scalo, J. 1998, in *Astronomical Society of the Pacific Conference Series*, Vol. 142, *The Stellar Initial Mass Function (38th Herstmonceux Conference)*, ed. G. Gilmore & D. Howell, 201
- Scalo, J. M. 1986, *FCPh*, 11, 1
- Schneider, N., Bontemps, S., Simon, R., et al. 2006, *A&A*, 458, 855, doi: [10.1051/0004-6361:20065088](https://doi.org/10.1051/0004-6361:20065088)
- Schneider, N., Simon, R., Bontemps, S., Comerón, F., & Motte, F. 2007, *A&A*, 474, 873, doi: [10.1051/0004-6361:20077540](https://doi.org/10.1051/0004-6361:20077540)
- Sharma, S., Pandey, A. K., Ogura, K., et al. 2008, *AJ*, 135, 1934, doi: [10.1088/0004-6256/135/5/1934](https://doi.org/10.1088/0004-6256/135/5/1934)
- . 2006, *AJ*, 132, 1669, doi: [10.1086/507094](https://doi.org/10.1086/507094)
- Sharma, S., Pandey, A. K., Ojha, D. K., et al. 2017, *MNRAS*, 467, 2943, doi: [10.1093/mnras/stx014](https://doi.org/10.1093/mnras/stx014)
- . 2007, *MNRAS*, 380, 1141, doi: [10.1111/j.1365-2966.2007.12156.x](https://doi.org/10.1111/j.1365-2966.2007.12156.x)
- Sharma, S., Pandey, A. K., Pandey, J. C., et al. 2012, *PASJ*, 64, 107, doi: [10.1093/pasj/64.5.107](https://doi.org/10.1093/pasj/64.5.107)

- Shevchenko, V. S., Ibragimov, M. A., & Chenysheva, T. L. 1991, *Soviet Ast.*, 35, 229
- Siess, L., Dufour, E., & Forestini, M. 2000, *A&A*, 358, 593
- Skrutskie, M. F., Cutri, R. M., Stiening, R., et al. 2006, *AJ*, 131, 1163, doi: [10.1086/498708](https://doi.org/10.1086/498708)
- Spitzer, Jr., L., & Hart, M. H. 1971, *ApJ*, 164, 399, doi: [10.1086/150855](https://doi.org/10.1086/150855)
- Stetson, P. B. 1987, *PASP*, 99, 191, doi: [10.1086/131977](https://doi.org/10.1086/131977)
- . 1990, *PASP*, 102, 932, doi: [10.1086/132719](https://doi.org/10.1086/132719)
- Stetson, P. B. 1992, in *Astronomical Society of the Pacific Conference Series*, Vol. 25, *Astronomical Data Analysis Software and Systems I*, ed. D. M. Worrall, C. Biemesderfer, & J. Barnes, 297
- Tan, J. C., Beltrán, M. T., Caselli, P., et al. 2014, in *Protostars and Planets VI*, ed. H. Beuther, R. S. Klessen, C. P. Dullemond, & T. Henning, 149
- Taylor, A. R., Gibson, S. J., Peracaula, M., et al. 2003, *AJ*, 125, 3145, doi: [10.1086/375301](https://doi.org/10.1086/375301)
- Thompson, M. A., Urquhart, J. S., Moore, T. J. T., & Morgan, L. K. 2012, *MNRAS*, 421, 408, doi: [10.1111/j.1365-2966.2011.20315.x](https://doi.org/10.1111/j.1365-2966.2011.20315.x)
- Tibaldo, L., & Grenier, I. A. 2013, *Nuclear Physics B Proceedings Supplements*, 239, 70, doi: [10.1016/j.nuclphysbps.2013.05.011](https://doi.org/10.1016/j.nuclphysbps.2013.05.011)
- Tody, D. 1986, *Society of Photo-Optical Instrumentation Engineers (SPIE) Conference Series*, Vol. 627, *The IRAF Data Reduction and Analysis System*, ed. D. L. Crawford, 733
- . 1993, *Astronomical Society of the Pacific Conference Series*, Vol. 52, *IRAF in the Nineties*, ed. R. J. Hanisch, R. J. V. Brissenden, & J. Barnes, 173
- Turner, D. G. 1976, *AJ*, 81, 1125, doi: [10.1086/111994](https://doi.org/10.1086/111994)
- Uchiyama, Y., Takahashi, T., Aharonian, F. A., & Mattox, J. R. 2002, *ApJ*, 571, 866, doi: [10.1086/340121](https://doi.org/10.1086/340121)
- Vansevicius, V. 1992, *Baltic Astronomy*, 1, 31, doi: [10.1515/astro-1992-0106](https://doi.org/10.1515/astro-1992-0106)
- Walker, G. A. H., & Hodge, S. M. 1968, *PASP*, 80, 290, doi: [10.1086/128631](https://doi.org/10.1086/128631)
- Watson, C., Hanspal, U., & Mengistu, A. 2010, *ApJ*, 716, 1478, doi: [10.1088/0004-637X/716/2/1478](https://doi.org/10.1088/0004-637X/716/2/1478)
- Wendker, H. J., Schramm, K. J., & Dieckvoss, C. 1983, *A&A*, 121, 69
- Whittet, D. C. B., ed. 2003, *Dust in the galactic environment*
- Whitworth, A. P., Bhattal, A. S., Chapman, S. J., Disney, M. J., & Turner, J. A. 1994, *MNRAS*, 268, 291, doi: [10.1093/mnras/268.1.291](https://doi.org/10.1093/mnras/268.1.291)
- Wright, E. L., Eisenhardt, P. R. M., Mainzer, A. K., et al. 2010, *AJ*, 140, 1868, doi: [10.1088/0004-6256/140/6/1868](https://doi.org/10.1088/0004-6256/140/6/1868)
- Yadav, R. K. S., Sariya, D. P., & Sagar, R. 2013, *MNRAS*, 430, 3350, doi: [10.1093/mnras/stt136](https://doi.org/10.1093/mnras/stt136)
- Zinnecker, H., & Yorke, H. W. 2007, *ARA&A*, 45, 481, doi: [10.1146/annurev.astro.44.051905.092549](https://doi.org/10.1146/annurev.astro.44.051905.092549)

Table 1. Log of optical observations with the 104-cm Sampurnanand telescope, Nainital.

Date of observations/Filter	Exp. (sec) \times No. of frames
SA98	
04 November 2005	
<i>U</i>	$180 \times 1, 300 \times 9$
<i>B</i>	$120 \times 3, 180 \times 8$
<i>V</i>	$60 \times 8, 120 \times 3$
<i>R_c</i>	$30 \times 9, 60 \times 3$
<i>I_c</i>	$30 \times 10, 60 \times 2$
NGC 6910(Center)	
<i>U</i>	$60 \times 3, 300 \times 3$
<i>B</i>	$30 \times 3, 180 \times 3$
<i>V</i>	$60 \times 3, 120 \times 3$
<i>R_c</i>	$10 \times 3, 60 \times 3$
<i>I_c</i>	$10 \times 3, 60 \times 3$
NGC 6910(Center)	
13 June 2005	
<i>U</i>	$300 \times 3, 1200 \times 3$
<i>B</i>	$300 \times 3, 900 \times 3$
<i>V</i>	$10 \times 3, 60 \times 3, 900 \times 3$
<i>R_c</i>	$10 \times 1, 300 \times 4$
<i>I_c</i>	$0 \times 1, 1 \times 1, 2 \times 1, 5 \times 3$
NGC 6910(F1)	
28 September 2006	
<i>U</i>	$300 \times 4, 1200 \times 3$
<i>B</i>	$60 \times 3, 900 \times 3$
<i>V</i>	$10 \times 1, 60 \times 3, 900 \times 3$
<i>I_c</i>	$10 \times 3, 300 \times 4$
NGC 6910(F2)	
29 September 2006	
<i>U</i>	$300 \times 2, 1200 \times 2$
<i>B</i>	$60 \times 3, 900 \times 2$
<i>V</i>	$60 \times 3, 900 \times 2$
<i>I_c</i>	$10 \times 2, 60 \times 3, 300 \times 4$
NGC 6910(F3)	
15 June 2005	
<i>U</i>	$60 \times 1, 300 \times 3, 1200 \times 3$
<i>B</i>	$10 \times 3, 60 \times 3, 900 \times 3$
<i>V</i>	$30 \times 3, 60 \times 1, 900 \times 3$
<i>I_c</i>	$10 \times 3, 20 \times 1, 60 \times 1, 300 \times 4$
NGC 6910(F4)	
26 September 2006	
<i>U</i>	300×3
<i>B</i>	120×4
<i>V</i>	120×3
<i>I_c</i>	$10 \times 3, 30 \times 1, 300 \times 4$
NGC 6910(F4)	
27 September 2006	
<i>U</i>	$300 \times 3, 1200 \times 3$
<i>B</i>	$60 \times 3, 900 \times 3$
<i>V</i>	$60 \times 3, 900 \times 3$

Table 2. List of surveys adopted in present work (NIR to radio wavelength).

Survey	wavelength(s)	Resolution	References
Two Micron All Sky Survey (2MASS)	1.25-2.2 μm	$\sim 2''.5$	Skrutskie et al. (2006)
UKIRT NIR Galactic Plane Survey (GPS)	1.25-2.22 μm	$\sim 0''.8$	Lawrence et al. (2007)
Spitzer Spitzer Enhanced Imaging Products (SEIP)	3.6, 4.5, 5.8 and 8 μm	$\sim 2'', \sim 2'', \sim 2'', \sim 2''$	^a
Wide-field Infrared Survey Explorer (WISE)	3.4, 4.6, 12 and 22 μm	$\sim 6''.1, \sim 6''.4, \sim 6''.5, \sim 12''$	Wright et al. (2010)
Spitzer MIPS Inner Galactic Plane Survey (MIPSGAL)	24 μm	$\sim 6''$	Carey et al. (2005)
Herschel Infrared Galactic Plane Survey (Hi-GAL)	70, 160, 250, 350, 500 μm	$\sim 5''.8, \sim 12'', \sim 18'', \sim 25'', \sim 37''$	Molinari et al. (2010)
Planck polarization data	850 μm	$\sim 294''$	Planck Collaboration et al. (2014)
CO survey Archive	2.6 mm	$\sim 8'.4$	Dame et al. (2001)
NRAO VLA Sky Survey (NVSS)	21 cm	$\sim 46''$	Condon et al. (1998)
Canadian Galactic Plane Survey (CGPS)	21 cm, 74 cm	$1' \times 1' \text{ csc}\delta, 3'.4 \times 3'.4 \text{ csc}\delta$	Taylor et al. (2003)
GAIA DR2 (magnitudes, Parallax and Proper motion)	330-1050nm	0.4 mas	Gaia Collaboration et al. (2018a,b)

^a: <https://irsa.ipac.caltech.edu/data/SPITZER/Enhanced/SEIP/overview.html>

Table 3. Sample of the 128 cluster members identified through their *Gaia* proper motion data. Complete table is available in the electronic form only.

ID	α_{J2000} (deg)	δ_{J2000} (deg)	V (mag)	B (mag)	I (mag)	R (mag)	U (mag)	Parallax (mas)	$\mu_\alpha \cos(\delta)$ (mas yr ⁻¹)	μ_δ (mas yr ⁻¹)	G (mag)	$(G_{BP} - G_{RP})$ (mag)	P_μ (%)
1	305.888133	40.693244	18.376 \pm 0.011	19.838 \pm 0.015	16.211 \pm 0.010	-	-	0.753 \pm 0.131	-2.706 \pm 0.148	-5.341 \pm 0.197	17.450	2.080	98
2	305.898745	40.707285	19.526 \pm 0.014	21.124 \pm 0.033	17.243 \pm 0.010	-	-	0.374 \pm 0.216	-2.408 \pm 0.225	-5.536 \pm 0.323	18.504	2.145	96
3	305.875944	40.712293	19.277 \pm 0.013	20.818 \pm 0.023	16.937 \pm 0.013	-	-	0.453 \pm 0.161	-2.974 \pm 0.183	-5.727 \pm 0.247	18.245	2.167	81
4	305.797771	40.716103	19.653 \pm 0.013	21.479 \pm 0.052	17.105 \pm 0.060	18.307 \pm 0.027	-	0.389 \pm 0.205	-2.527 \pm 0.306	-5.285 \pm 0.314	18.427	2.377	96

Table 4. A summary of the physical parameters of the cluster.

Reference	R_{cl} (arcmin)	Age (Myr)	Distance modulus (mag)	R_V	$E(B - V)$ (mag)
Present study ($UBVRI$)	5.5	4.5 \pm 2.5	11.18 \pm 0.12	3.75 \pm 0.02	0.95 \pm 0.10
Delgado & Alfaro (2000, UBV)	—	6.5 \pm 3.0	11.2 \pm 0.2	3.1 \pm 0.1	1.02 \pm 0.13
Kolaczowski et al. (2004, VI)	—	6.0 \pm 2.0	11.0 \pm 0.3	—	1.19 \pm 0.21

Table 5. The mass function slope for two sub-regions and for the whole cluster region in the given mass range.

Mass range (M_\odot)	Mass Function slopes (Γ)		
	Core region	Corona region	Cluster region
24.86 – 0.8	-0.42 \pm 0.20	-0.69 \pm 0.14	-0.74 \pm 0.15
24.86 – 2.3	-0.38 \pm 0.39	-0.54 \pm 0.28	-0.58 \pm 0.25